ABSTRACT

O'CONNELL, MATTHEW. Assessment of Interfacial Adhesives used in Flexible Thin Film Encapsulation. Under the direction of Dr. Brendan O'Connor.

The development of solution processable polymer semiconductors have enabled organic photovoltaics (OPVs) to possess lightweight and flexible attributes. Fabrication of OPVs on polymer substrates enables unique flexible applications such as wearable electronics, building integrated photovoltaics, or avionics. However, the materials used in OPVs degrade over time upon exposure to the combination of irradiation, moisture, oxygen, and mechanical stresses. Degradation due to atmospheric permeation should be considered the main contributing factor to the accelerated loss of OPV performance. Encapsulation between multilayer thin film barriers provides significant protection from the ingress of moisture and oxygen into the device stack. Laminating the barrier films onto OPVs through the use of interfacial adhesives is a promising flexible encapsulation strategy but must demonstrate robust stability because flexible applications may endure repeated compressive, tensile, and torsional stresses. The influence of interfacial adhesives on the mechanical stability of flexible OPV encapsulation is narrowly defined. This investigation considers the robust performance of common flexible encapsulation architectures under bending and peeling stresses. Full coverage, perimeter, and combined application of the interfacial adhesives are investigated to inform which encapsulation architecture is most robust and reliable. Optimization of the interfacial adhesive layer in regard to the quality, thickness, and processing conditions is considered. It is determined that interfacial adhesives that cover the entire surface area of the device and substrate demonstrate consistent mechanical stability. Epoxy and acrylic adhesives are deemed as the best performing adhesives. The mechanical test that accurately informs mechanical reliability is determined as a bending test combined with the optical calcium test, traditionally used to define the barrier performance of the adhesive layer.

Assessment of Interfacial Adhesives used in Flexible Thin Film Encapsulation

by
Matthew Patrick O'Connell

A thesis submitted to the Graduate Faculty of
North Carolina State University
in partial fulfillment of the
requirements for the degree of
Master of Science

Mechanical Engineering

Raleigh, North Carolina
2023

APPROVED BY:

Dr. Brendan O'Connor
Committee Chair

Dr. Arun Kota

Dr. Lokendra Pal

DEDICATION

I would like to dedicate my work to my loving family. Their support along my academic career has enabled me to pursue opportunities I would not have otherwise envisioned for myself and it is because of their guidance and wisdom that I was able to pursue higher education.

BIOGRAPHY

Matthew O'Connell is from Germantown, MD and pursued his Bachelor's Degree in Mechanical Engineering from the University of Maryland, College Park. Due to the turbulent times during covid and the uncertainty of his desires in the professional industry, he pursued his higher education at NC State University in Raleigh, NC. This was the first time he had moved away from home and his experience has prepared him to begin his professional career with Siemens in the eMobility Project Management Office in Wendell, NC. He will serve as a Service Project Manager where he will be overseeing the maintenance and service of existing and new installations of DC and AC electric vehicle charging equipment. His research has established his passion for overseeing project implementation and he is grateful for the opportunity to learn about the promising applications of organic electronics.

ACKNOWLEDGMENTS

I want to thank Dr. Brendan O'Connor for his support and guidance during my time at NC State. His dedication to research and ability to guide me along my path has helped me develop into a better academic and professional. I would also like to thank Harry Shrickx and Shafe Al Abdullah for their support and valuable lessons they shared with me, as well as all of the time they spent training me. Thank you to Dr. Harald Ade for the opportunity to use the shared ORaCEL research space.

TABLE OF CONTENTS

LIST OF TABLES

LIST OF FIGURES

CHAPTER 1: Introduction

1.1 Motivation and Background

1.1.1 Flexible OPVs

Society is in the process of transitioning to more sustainable and eco-friendly sources of energy as the reliance on high carbon-emitting solutions has proven harmful to the stability of our environment[1]. Traditional crystalline silicon (c-Si) photovoltaics boast higher efficiencies and longer term stability than the emerging organic photovoltaic (OPV) technologies[2] . However, with the emergence of OPVs, a wide range of potential unique applications exists. OPV's inherent lightweight, flexible, and low cost characteristics create addressable markets such as wearable devices, agrivoltaics, space applications, and avionics [3,4,5,6]. The robustness of flexible organic photovoltaics is critical to the feasibility of their application within these markets. The ability to operate at optimal efficiency for prolonged durations whilst conforming to non-uniform surfaces and withstanding variable high stress conditions is necessary to meet commercialization standards.

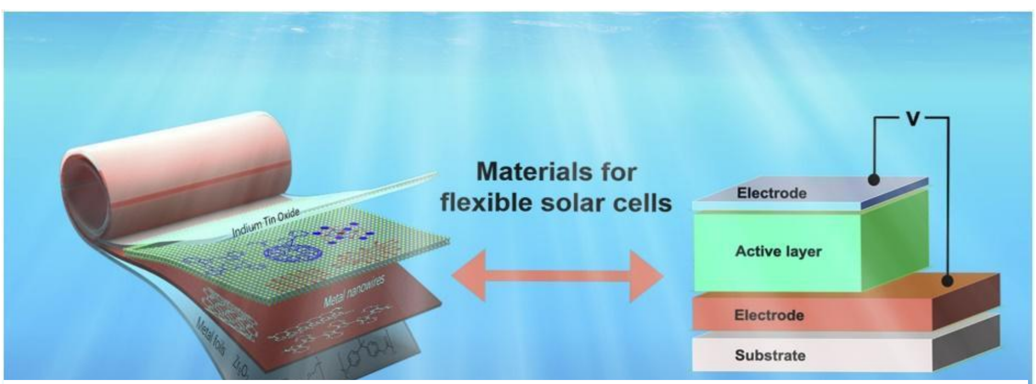

Figure 1. A representation of a flexible solar cell and its device stack structure. Adapted from Li et al. *Mater. Reports Energy* **2021**, *1* (1), 100001.[7]

The ability to achieve high power conversion efficiencies (PCE) using highly flexible device structures has been demonstrated and continues to aim higher [8,9,10]. Figure 1 demonstrates a flexible OPV structure. The functional stack of OPVs is comprised of blocking or transport layers combined with the light harvesting active layer to form a total thickness that ranges to just a few hundred nanometers [11]. These stacks are commonly deposited onto polymer substrates such as polyethylene terephthalate (PET), polyimide (PI), and polyethylene naphthalate (PEN) for their lightweight attributes, low cost supply and compatibility with high throughput processing [6,11]. Polymer substrates increase the final thickness of the devices however remaining relatively thin between a few hundred microns. Polymer substrates used in flexible OPVs are known to be highly permeable to oxygen and moisture [12, 13]. This is due to their high molecular chain mobility which allows for their flexible and conformal applications. However, this high rate of permeation has been shown to accelerate the degradation of the functional parameters of OPVs including the short-circuit current (Jsc), open-circuit voltage (Voc), and fill factor (FF) [7, 12, 13]. This ultimately degrades the power conversion efficiency (PCE) of OPVs dramatically limiting their lifetimes. Solutions to prevent the ingress of moisture and oxygen are the deposition of thin metal oxides or the formation of alternating organic/inorganic material multilayers onto the devices. However, considering how these solutions impact the flexibility of the device should not be neglected. Many efforts have been made to promote long-term stability of the flexible OPVs through optimization of the functional layers and photoactive layer materials [14, 15, 16], surface treatments of the functional layer, and processing conditions during fabrication [17, 18]. Consideration of the extrinsic and intrinsic factors that affect the stability of flexible OPVs will inform the most suitable solutions to enhance their operational lifetimes.

1.1.2 Device Stability

Organic photovoltaic (OPV) device stability is critical for its practical implementation into industrial or commercial applications. The general consensus among researchers and industry professionals is that OPVs must meet the fundamental requirements of PCE greater than 18% and maintain this performance at lifetimes greater than 10 years [19, 20]. While the performances of flexible OPVs have achieved PCEs that exceed this minimum requirement, their stability outside of inert lab controlled atmospheres has proven quite challenging [19, 21]. The degradation principles that diminish the PCEs and accelerate the loss of functionality of OPVs must be understood in order to achieve the unique capabilities OPVs offer in the solar energy industry.

Organic photovoltaics (OPVs) are impacted by several mechanisms of degradation that affect their performance over time. Figure 2 illustrates the main factors that combine to influence the stability of OPVs, including light, temperature, atmosphere, and mechanical stress [12]. These factors can cause degradation that is classified as either intrinsic or extrinsic. Intrinsic degradation

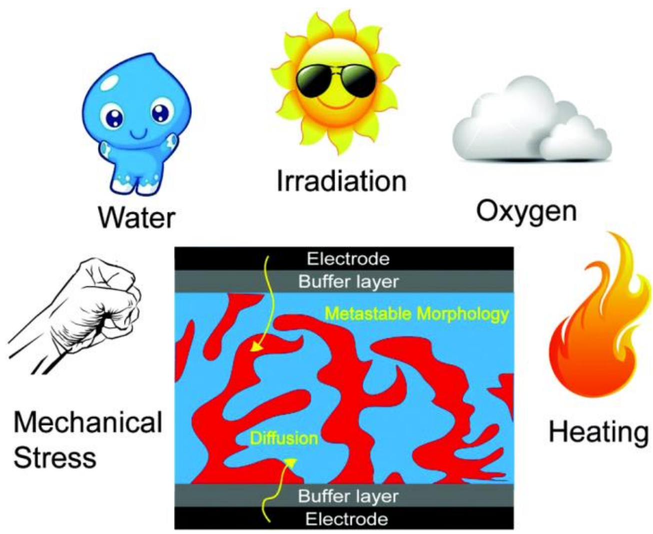

Figure 2. Extrinsic and Intrinsic Factors impacting the stability of OPVs. Adapted from Cheng et al. *Chem. Soc. Rev.* **2016**, *45* (9), 2544–2582. [12]

involves morphological or interfacial changes to the transport layers, active layer, or metal electrodes. This can include phase segregation of the photoactive layer (PAL) materials, phase separation at the interface of the active layer and hole transport layer (HTL), and interdiffusion of the metal electrode into the active layer [13, 21]. Each of these chemical and physical reactions contribute to the loss of performance and stability of OPVs. However, they are strongly influenced and often accelerated by extrinsic factors like elevated temperatures and permeated atmospheric molecules [13, 22].

Extrinsic degradation mechanisms are considered environmental conditions that impact OPVs such as fluctuations in temperature, light intensity, atmospheric conditions, static and cyclical mechanical stresses, and even impact stresses from weather events such as hail [22]. Temperature and light can be grouped together as extrinsic factors, as the operational temperature of OPVs increases with continuous irradiation. Irradiation-induced instability is described by photochemical and photophysical reactions of the PAL, buffer layers, and PAL/electrode interface [12, 13]. Photochemical reactions, particularly photo-oxidation, are predominant and can cause changes in the metastable structure of the PAL, leading to decreased photo absorption, catalysis of sub-bandgap materials formation, alteration of energetic disorder, changes in energy levels of electron donors and acceptors, and formation of radicalized cations on the polymer chain, resulting in a relaxed charge transfer state [12, 13]. Moreover, depending on the glass-transition temperature (Tg) of the PAL materials, elevated operational temperature may induce increased chain mobility, leading to PAL aggregation, reorganization, or crystallization. The combination of these photophysical and photochemical reactions results in reduced exciton generation, dissociation, and charge transfer due to altered donor/acceptor (D/A) interfaces, significantly impacting the performance of OPVs [13]. Similarly, the buffer layers and PAL/electrode interface are also susceptible to extrinsically induced reactions that further degrade the performance and stability of OPVs. The predominant cause of loss of performance can be attributed to atmospheric permeation into the device stack [23, 22]. As moisture diffuses through the device stack, metal oxide layers can form at the interfaces between the electrode and active layer reducing the conductivity and performance of the device [12]. Inverted device stacks using silver (Ag) as the conductive electrode is a widely used solution as it is less reactive to oxygen and water. Drakonis et al. demonstrate the improved stability of inverted devices with silver electrodes compared to conventional devices with aluminum at the same testing conditions [24]. It is observed that after one hour in air, the inverted structures maintain 95% of their power conversion efficiency (PCE) while the conventional structures drop to only 20% of their original PCE. While permeation orthogonal to the device stack may be reduced significantly, there is still significant permeation through the edges of device stack layer. Edge permeation will therefore induce the same reactions, degrading the interfaces of the layers and diffusing through the bulk of the materials initiating photo-oxidative reactions.

The transport layers also demonstrate high sensitivity to atmospheric permeation. As moisture and oxygen ingress the device combined with the exposure to light, photo-oxidation occurs degrading the surfaces and bulk morphology of the buffer layers [25]. Commonly used hole transport layer material PEDOT:PSS has a hygroscopic nature thereby readily absorbing water and reducing conductivity. Arredondo et al. demonstrate that the presence of oxygen combined with UV exposure decreases the conductivity of PEDOT:PSS, establishing the importance of controlled fabrication and processing conditions [26].

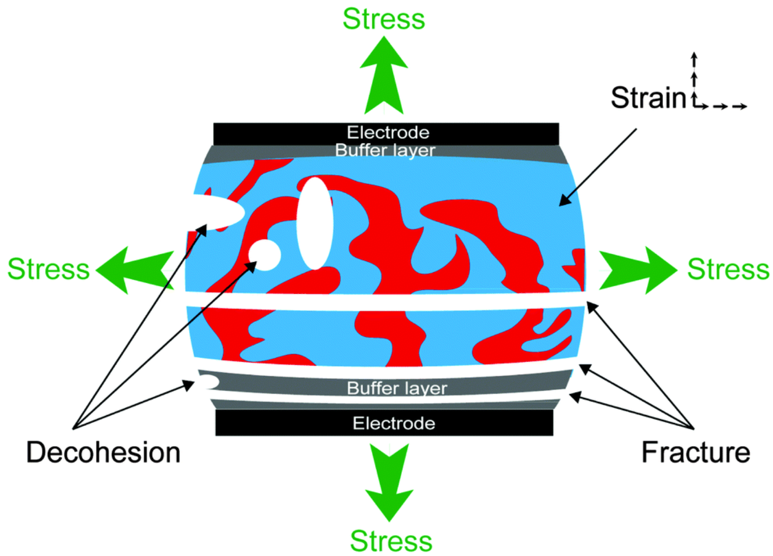

Figure 3. Mechanical stress conditions that induce failure mechanisms in the device stack. Adapted from Cheng et al. *Chem. Soc. Rev.* **2016**, *45* (9), 2544–2582. [12]

Extrinsic factors that may be difficult to mitigate such as temperature, light, and atmosphere affect the intrinsic stability of the organic/inorganic materials of OPVs. However, flexible OPVs must withstand compressive, tensile, and torsional stresses due to applied loading conditions such as bending, stretching, and twisting. These induced stresses may result in failures such as fracture or delamination of the interlayers due to their generally low adhesive and cohesive strengths. It has been demonstrated that the application of tension on the material layers may induce large enough strains (Figure 3) that damage the structure and degrade the performance of the OPV [12]. Delamination or fracture within the device stack, or the encapsulation layers, ultimately results in the failure of OPVs. Thus, development of practical testing conditions that simulate the various loading conditions flexible OPV applications will undergo is of interest. Application of these testing conditions should be used to evaluate the mechanical reliability of flexible OPVs and may inform the stability and design considerations of OPVs.

Flexible OPVs face many challenges in regard to the stability of the materials and long term operational performance. Extrinsic factors induce and often accelerate the intrinsic instability of the organic/inorganic material layers. Preventing the exposure to humidity and oxygen is of upmost importance to long-term OPV stability. The introduction of a barrier layer as a method to prolong or even prevent atmospheric permeation is necessary. Existing and novel solutions in the food packaging industry may be adopted to flexible OPVs as the preservation of perishable foods has continued to improve [27]. However, the sensitivity and robustness of these packaging solutions may ultimately need to be adapted with appropriate material selection and scalable fabrication methods. The sensitivity of the OPVs functionality is much more stringent than the freshness of packaged food as will be discussed. Mechanically robust solutions paired with strong barrier properties are available but their suitability and impact on the flexible performance of OPVs must be reviewed [28].

1.1.3 Encapsulation Materials and Barrier Types

The materials used in OPV fabrication are highly sensitive to oxygen and water. They necessitate the implementation of a barrier solution to prevent their accelerated degradation. Encapsulation is defined as the protection of solar cells through application of gas-barrier materials to delay contact between the device and ambient atmosphere. Glass is understood to be the ideal encapsulation material due to its inherent impermeable and highly transparent characteristics. It is commonly used in solar applications where the flexibility of the solar cell is trivial and has proven to be an effective barrier in organics, perovskites, and traditional silicon or cadmium solar cells [22, 29]. The scope of this investigation concerns the application of flexible OPV encapsulation, thereby eliminating glass and assessing alternative solutions that provide flexibility, low permeability of water and oxygen, blocking of harmful UV exposure, thermal stability, and mechanical resilience.

Previous investigations have identified that for OPVs, the water vapor transmission rate (WVTR) of $10^{-3} – 10^{-6}$ g m^{-2} d^{-1} and oxygen transmission rate (OTR) of $10^{-3} – 10^{-6}$ cm^3 m^{-2} d^{-1} are within an acceptable range of permeability (22, 30, 31). Cros et al. conducted accelerated lifetime experiments on encapsulated OPVs under 38 C$^{\circ}$ and 100 % relative humidity (RH) conditions, while measuring the amount of diffused water over time. They considered a 50% loss of the PCE as critical loss of functionality and determined that a water vapor transmission rate less than 10^{-3} corresponded to an extrapolated lifetime of several years (31). However, their determination is under the assumption that the WVTR was under focus and no distinction between the effects of the oxygen and irradiation were considered. Therefore, the OTR is assumed to require the same performance. Figure 4 demonstrates how this range of permeability compares to other technologies sensitive to atmospheric permeation with OLEDs requiring the lowest range and food packaging being much higher.

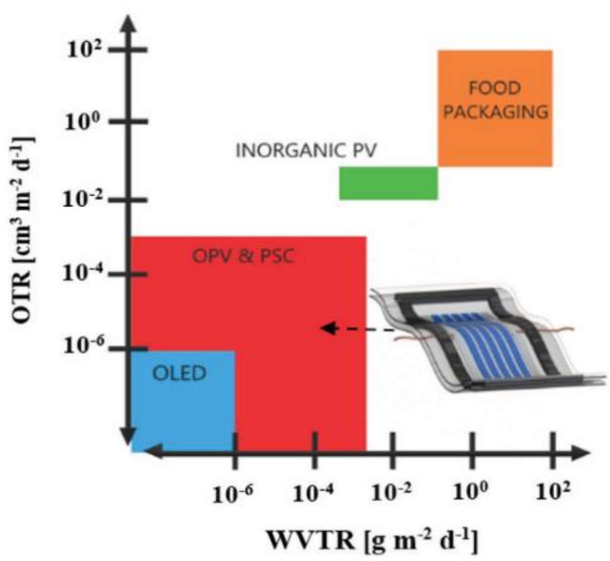

Figure 4. Demonstration of the range of barrier requirements for OPV encapsulation. Adapted from Sutherland et al. *Adv. Energy Mater.* **2021**, *11* (34). (22)

The water vapor and oxygen transmission rates can be characterized as the speed at which water and oxygen molecules diffuse through a defined area of material. Illustrated in Table 1, existing quantitative methods utilized to determine the permeability of barriers as well as more unique approaches have been reviewed and summarized by Kempe et al [41].

Table 1. Existing commercial and research designed permeation rate test methods for encapsulation barriers. [41]

Test Method	References or Standards	Process	Range ($g/m^2/day$)	Strengths/limitations
Isostatic	ASTM F1249 [60]	Diffusion cell using coulometric moisture sensor or infrared sensor	$5 \, x \, 10^{-4} - 200$	• Commercial availability • Wide range of environmental control • Intermediate sensitivity and limited throughput
HTO/radioactive tracer	Dameron [32], Dunkel [33]	Diffusion cell with detection of moisture doped tritium through ionization chamber	$10^{-8} - 10$	• High sensitivity • No commercial standard
Optical Ca Test	Graff [34], Boldrighini [35]	Monitoring calcium oxide formation through visual inspection	$10^{-6} - 10$	• High sensitivity • Wide range of environmental control and high throughput • High capital investment • Time intensive/no standard
Mass spectroscopy	Zhang [36], Renade [37]	Diffusion cell with residual gas analyzer	$10^{-7} - 10$	• High sensitivity • Monitoring of moisture and other molecules • High capital investment • No commercial standard
Electrical Ca Test	Paetzold[38], Choi[39], Song[40]	Monitoring calcium oxide formation through change in electrical resistivity	$10^{-7} - 10$	• High sensitivity • Wide range of environmental control and high throughput • High capital investment • Time intensive/no standard

Characterization of a flexible encapsulant barrier is necessary in order to determine the classification and comparison of high performing materials. The barrier performance of the flexible encapsulants determines the effectiveness of the barrier at preventing or prolonging an OPV's exposure to water and oxygen. It is critical to understand which commonly seen encapsulation materials meet the required barrier performance requirements. The mechanical reliability of the barrier should not be neglected, and the robustness can be assessed by simulating practical stress conditions through various mechanical tests. However, evaluative methods for informing the mechanical reliability of scalable flexible encapsulation strategies must first be defined. Understanding the reliability of existing flexible encapsulation solutions may inform design considerations that help select the materials and methods compatible with high throughput processing methods.

Current flexible encapsulation materials and methods require high performing barrier properties as well compatibility with scalable fabrication. The common barrier materials used in flexible OPV encapsulation are often polymer based due to the benefits polymers provide in flexible applications [7, 22]. Previously mentioned, thin polymers generally have poor barrier properties due to their increased molecular chain mobility. However, significant efforts have been made to combine the intrinsic flexibility and compatibility of polymers with inorganic materials to improve the barrier performance. The development of thin organic/inorganic multilayered films and polymer nanocomposites present promising candidates for effective flexible OPV encapsulation.

Thin Film Barrier Encapsulation (TFE):

Thin film barriers consist of either a single layer or multi-layered structure of organic/inorganic materials. Inorganic materials such as aluminum oxide (Al_2O_3), silicon oxide (SiO_x), and titanium oxide (TiO_2) can be deposited via atomic layer deposition (ALD) or chemical vapor deposition (CVD) onto organic materials such as polyethylene terephthalate (PET), polydimethylsiloxane (PDMS), or polyethylene naphthalate (PEN) [22, 42]. However, use of a single barrier layer of organic or inorganic material does not provide sufficient prevention of oxygen and water permeation. While thin layers of inorganic materials have demonstrated the ability to prolong the lifetime of OPVs and achieve barrier performance within the required range shown in

Figure 4, they are subject to common defects such as pinholes and may crack during bending [22, 42]. Inserting polymers between layered inorganic materials has been proven to improve the flexibility under mechanical stresses and effectively establishes an extended diffusion path length. For example, Lay et al. developed a SiN_x – SiO_x – parylene multilayer structure for OPV encapsulation demonstrating 4.74 x 10^{-5} g/m^2/day after 1000 bending cycles to 10 cm [43]. Following ISOS-D-2 protocol, the barrier performance was measured at 25C and 90% RH [44]. The fabrication process involved depositing the multilayer stack onto polycarbonate substrates through inductively coupled plasma chemical vapor deposition (ICPCVD) which allows for high quality low-temperature (<150C) processing of silicon materials. The WVTR reported was determined by testing a layer of calcium's resistivity over time across a multilayer stack including 3 pairs of 50 nm SiO_x/100 nm SiN_x followed by a 700 nm parylene layer as the bottom barrier, and a top barrier including a 1000 nm parylene layer.

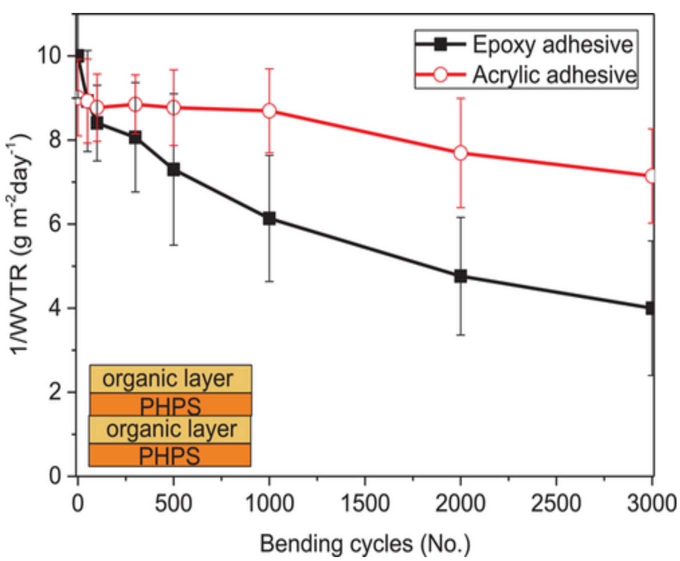

Figure 5. WVTR of sandwiched coatings of alternating PHPS/organic layers versus the number of bending cycles at a bending radius of 3 cm. The PHPS and organic layer thicknesses are respectively 170 nm and 5-10 µm. UV – curable Epoxy and acrylic adhesives were used as the inorganic layer. Adapted from Channa et al *Adv. Energy Mater.* **2019**, *9* (26), 1900598. [45]

Channa et al. further highlighted the potential of multilayers layer stacks by demonstrating a solution-processable barrier stack consisting of perhydropolysilazane (PHPS) and a varied organic interlayer deposited directly onto PET. Demonstrated in Figure X, using a solvent free acrylic adhesive as the organic interlayer shows less than a 10% loss of WVTR after 3000 bending cycles at a 3 cm bending radius.[(45)] It is asserted that the introduction of the organic interlayers provides a planarization effect which is interpreted to decrease the frequency of imperfections within the layers of PHPS. These imperfections are considered to contribute to the tensile cracks that form during bending, and they observe that PHPS layers deform in parallel with minimal defect interaction. While multilayer stacks are among the most promising candidates for flexible OPV encapsulation, there are limitations that pose challenges to their widespread implementation. Many of these limitations pertain to the throughput and practical use of thin film barriers. Existing thin film deposition technology such as ALD or CVD involves high temperature and under vacuum conditions, often requiring a series of expensive processing instruments and equipment. The cost and time needed to fabricate thin film barriers demonstrates the need for further understanding and development of multi-layer thin film deposition techniques that enable low temperature and open air processing conditions. Commercially available barrier films manufactured by companies such as Mitsubishi Chemical, 3M, or Opteria advertised by high barrier performances with WVTRs of $< 10^{-4}$, $< 5 \times 10^{-4}$, and 5×10^{-4} g m^{-2} day^{-1} can be utilized for lab scale testing while more practical and economical barrier fabrication techniques are developed [(22)]. However, pairing these films with a high performing barrier adhesive and compatible encapsulation method may prove to limit flexible performance of thin barrier films and should be investigated.

Polymer Nanocomposites:

Multilayered or stacked layers of polymers are used commercially in various packaging solutions, but they do not meet the ultra-high barrier requirements for OPVs. Polymer nanocomposite (PNC) films have emerged as a promising alternative to multilayer polymer films for the encapsulation of OPV devices. Fabrication of PNCs involves dispersing nanoscale particles, such as clay or metal oxide nanoparticles, into a polymer matrix to improve its mechanical, thermal, and barrier properties.[46] The application of PNCs to OPV encapsulation has been demonstrated to provide several advantages, including improved device stability, enhanced resistance to environmental degradation, and increased flexibility.[22] The incorporation of nanofillers helps improve the barrier performance by creating a more torturous path length for permeating gas molecules to travel. The torturous path length model is illustrated in Figure 6.

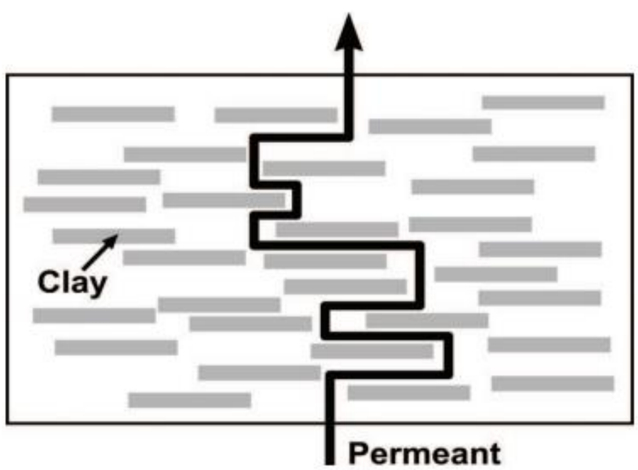

Figure 6. Illustration of permeating molecules traveling along a torturous path length of a polymer film with dispersed nanoclays. Adapted from *Advances in Diverse Industrial Applications of Nanocomposites*; Reddy, B., Ed.; IntechOpen: Rijeka, 2011.

The barrier performance of PNCs is dependent on the filler's material type, geometry, and level of dispersion within the polymer matrix. Additionally, the reinforcing effects of the fillers can be enhanced by optimizing the aspect ratio of the nanofillers. This is due to the matrix/filler interfacial adhesion or specific surface area which influences the fillers mobility within the matrix

[46]. Under flexible application, bending stresses may affect the original positioning of the fillers within the matrix. Interaction between the individual fillers during bending may create unwanted behaviors such as misalignment or decohesion of the fillers within the matrix. Therefore, the loading or weight percent (wt%) of the filler to polymer ratio must be considered.

Naturally occurring or commercially synthesized nanoclays such as Montmorillonite (MMT) or sodium-montmorillonite (Cloisite Na+), are widely used nanofillers due to their low cost, availability, and processability.[22, 47, 48] Seethamraju et al. investigated the barrier and mechanical performance of solution cast modified MMT Poly(vinyl alcohol-co-ethylene) films.[48] They tested films with varied clay content from 1 to 5 wt% and performed a series of mechanical and accelerated aging tests to evaluate the effectiveness of the barrier and its robustness. Each film demonstrated a percent elongation at break greater than 100% but decreased as the concentration increased as expected. However, the tensile yield strength and elongation at yield remained independent of loading content. Considering these findings, they assert the films as satisfactory conditions for flexible use case. The optimal clay content was determined to be 5 wt% which demonstrated a WVTR of 1×10^{-4} g m^{-2} day^{-1} at 35 °C and 95% RH. While demonstrating an effective improvement to neat polymer films, Seethamraju et al. recommended sandwiching these films between additional barrier films would likely be needed to meet the barrier requirements for OPV encapsulation. Therefore, investigation of the polymer clay nanocomposites as an interlayer or coating may satisfy the ultra-low barrier requirement. Gaume et al. demonstrates this possibility by coating thin PET films with PVA/MMT composites of varying weight percentages and investigated the transmittance and flexibility of the films.[47] They conclude that the optimal clay concentration to be 6 wt% with an associated transmittance of ~90% and WVTR of 7.86×10^{-6} at 38 °C and 100% RH testing conditions. It is also asserted that the coated films can be applied in flexible OPV encapsulation as the WVTR shows minimal loss after 10,000 bending cycles at 3 cm. While demonstrative of the ability to be applied in flexible applications, the range of mechanical reliability of PNCs is fairly limited and demonstrations of significant robustness have yet to be seen.

Inorganic oxide thin films exhibit excellent barrier properties but often tend to have defects such as pinholes or cleavages, diminishing their overall effectiveness in OPV encapsulation.[(22,42)] The inherent inflexibility of inorganics films can be improved by dispersion of metal oxide nanofillers within polymer matrices. Several investigations into the barrier, mechanical, and optical properties of metal oxide nanocomposite films have been conducted.[(22)] Barrier properties can be significantly improved through the incorporation of reactive metals such as magnesium and graphene oxides.[(49, 50)] However, metal oxides as a class of nanofillers have not yet been able to demonstrate barrier properties below the adequate range of $<10^{-5}$g $m^{-2}day^{-1}$.[(22, 49, 50)] Furthermore, to enable high flexibility and adequate mechanical reliability for flexible encapsulation, the thickness of the films must be reduced to the point at which the tortuosity effect is no longer impactful.

Engineered polymer nanocomposites show promise as a potential candidate for flexible encapsulation of OPVs. They demonstrate compatibility with high throughput R2R production thereby demonstrating economic feasibility. However, at this moment, PNCs need further development to be widely adopted. The barrier performance of PNCs has been demonstrated to provide significant improvement to neat polymer films alone, but their application is limited to coatings or interlayers. The combination of multiple nanofillers types such as metal oxides and clays has yet to be demonstrated and could be investigated as a potential solution to meet the highly sensitive barrier requirements of OPVs. However, the influence of nanofillers and their effect on the mechanical reliability and robustness of PNCs must be minimized.

1.1.4 Applying the encapsulation layer

The sensitivity of OPV devices to the ingress of moisture and oxygen must be prevented to prolong the device's operational lifetime and efficiency. Existing flexible OPV encapsulation methods demonstrate a promising solution to prevent extrinsic degradation factors. While effective barrier solutions have been developed to meet the sensitive barrier requirements of OPVs, the most flexible encapsulation strategies or methods must be identified. The pathways of permeation into a device stack may inform the design and selection of the most effective encapsulation strategy to employ. Figure 7 demonstrates the permeation pathways into a flexible encapsulated OPV that uses an edge seal barrier adhesive combined with a top and bottom barrier film to sandwich the device.

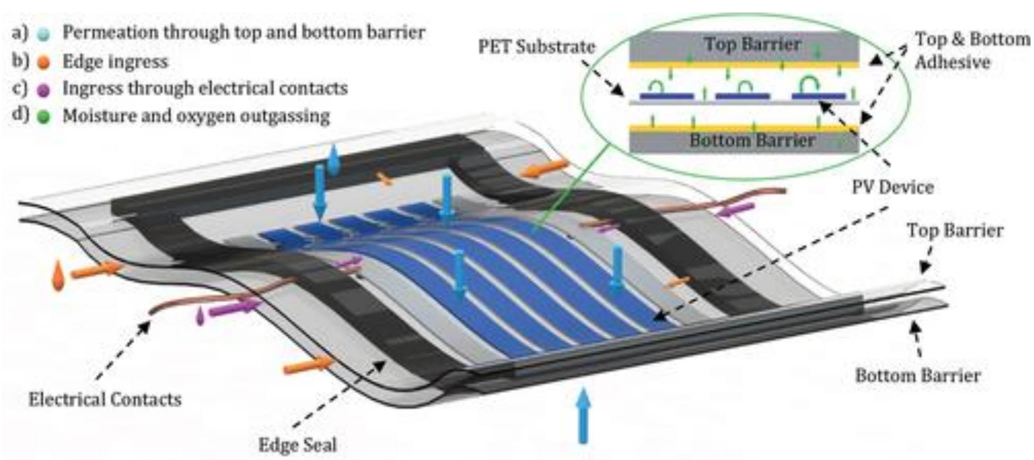

Figure 7. Demonstration of the permeation pathways into an encapsulated OPV device. a) Permeation orthogonal to the plane of top and bottom barrier. b) Ingress through edges of seal through the bulk adhesive and adhesive interface. c) Permeation through the electrical contact pathways. d) Outgassing of moisture and oxygen by encapsulation materials. Adapted from Sutherland et al. *Adv. Energy Mater.* **2021**, *11* (34), 1–32. [22]

Also relevant to the encapsulation strategy employed are the processing conditions which may interact with the highly sensitive photoactive layer and interlayer materials. Conditions such as the temperature, the level (ppm) of water and oxygen during encapsulation, and the mechanical stresses applied to the device stack must be considered. Traditionally, encapsulation must be performed in lab controlled inert atmospheres to prevent immediate degradation of the functional layers of the device stack. However, this may impact the scalability of the encapsulation strategies and limit the throughput fabrication of commercial products. Common ways to apply the encapsulation layer include lamination via a barrier adhesive and direct deposition onto the OPV. Industrial methods require higher throughput processing such as roll-to-roll lamination.

Lamination with barrier adhesives

Informed by glass to glass encapsulation seen in silicon photovoltaics and rigid OPV applications, thin film barrier encapsulation involves sandwiching an OPV between a front and back barrier material. Flexible thin film barrier encapsulation is also compatible with roll-to-roll technology, enabling the possibility of commercial scale up. The barriers can be bonded with barrier adhesive materials such as UV-curable adhesives, thermocurable adhesive, pressure sensitive adhesives. Adhesive sealing can be categorized into full device area coverage, edge or perimeter sealants, or a combination of the two. Figure 8 illustrates the common architectures seen in thin film barrier encapsulation.

Full device area coverage adhesives require high transparency and solvent free materials to enable optimal PCE and minimize any interaction with the sensitive PAL or interlayers.[22, 42, 51] Edge seal adhesives work to prevent the ingress of atmosphere through the perimeter edges of the encapsulation and have demonstrated significant effectiveness in prolonging permeation.[41, 52] However, permeation through the permeable top and bottom barrier is prevalent regardless of an edge sealant or full device area adhesive coverage. The lateral ingress through the edges of the encapsulation layers and along the electrical contact pathway has been shown to be mitigated through the integration of edge seal adhesives.(22, 51) Such adhesives generally include an integrated desiccant or getter material which is understood to react with the permeated molecules, preventing them from permeating into the device. Understanding the materials moisture and oxygen uptake capacity is critical to the effectiveness of these materials.

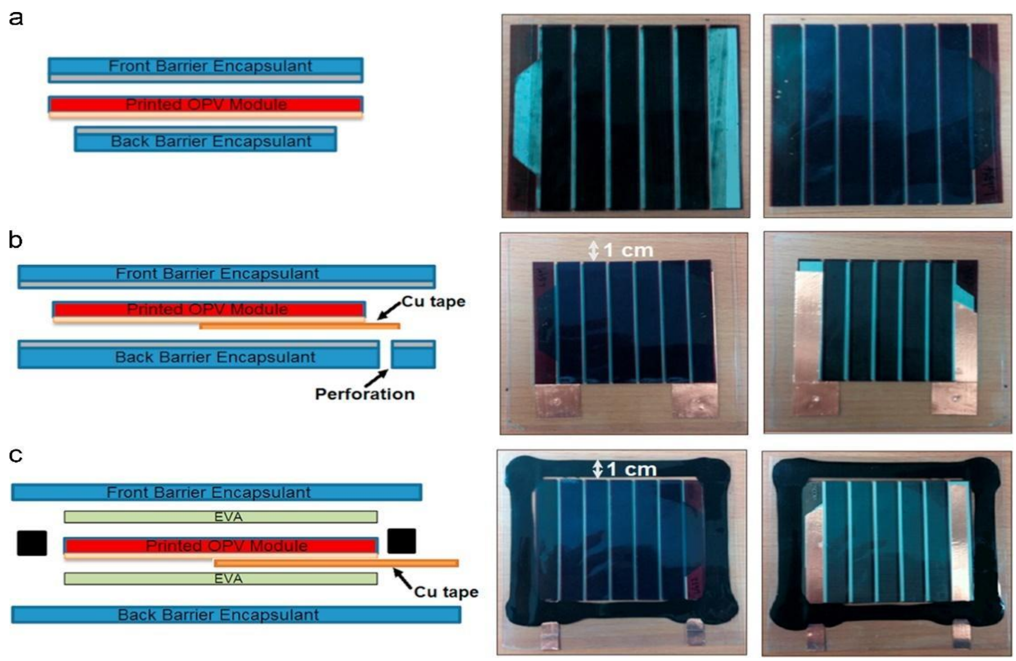

Figure 8. Partial, perforate, and complete encapsulation of an OPV. a) Partial encapsulation with the back encapsulant being narrower than the device to enable direct electrical contact. b) Perforated encapsulation with electrical contact being made by the copper tape via conducting adhesive. c) Complete encapsulation with thin film barriers bonded via full coverage interlayers combined with perimeter edge sealing. Adapted from Weerasinghe et al. *Sol. Energy Mater. Sol. Cells* **2016**, *155*, 108–116. (51)

Incorporating thin film barriers and barrier adhesives also creates the concern for material outgassing. Outgassing of polymeric encapsulants and adhesive materials was studied by Weerasinghe et al. in relation to its effect on OPV device stability.(51) They demonstrate that residual moisture retained in the barrier and adhesive materials can cause significant degradation of conventional and inverted OPV devices. Using impedance spectroscopy analysis, trace amounts of residual moisture as low as <20 ppm can significantly reduce device operational lifetimes. The significance of pre-conditioning barrier materials is highlighted by Figure 9. Weerasinghe et al. compare normalized current-voltage (J-V) parameters of OPV devices encapsulated with barrier materials conditioned initial moisture levels ranging from 1100 ppm to ≤1 ppm and find that devices ≤1 ppm experienced minimal changes in their parameters. This emphasizes the importance of preconditioning materials stored in ambient conditions to remove residual moisture content.

Thin film barrier encapsulation shows promise as the materials used are commercially accessible and the processing methods prove to be straightforward and economical. However, critical to the effectiveness of any flexible OPV encapsulation strategy is its durability and robustness. Combining the adhesive barrier and thin film barrier materials may create a mismatch in the material properties such as the elastic modulus or tensile strength. Understanding this

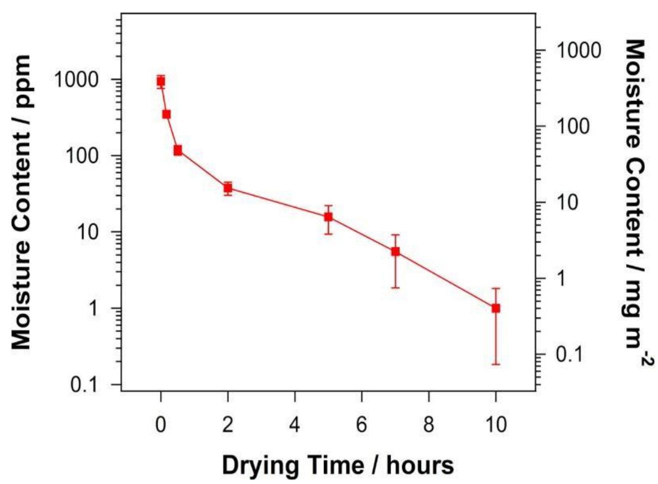

Figure 9. Moisture Content versus Drying Time/hours. Residual moisture content of Mitsubishi VIEWBARRIER thin film with an integrated pressure sensitive adhesive (PSA) layer as a function of conditioning time at 100C and ~10^{-3} mbar. Adapted from Weerasinghe et al. *Sol. Energy Mater. Sol. Cells* **2016**, *155*, 108–116. [51]

interaction will be critical to evaluating the mechanical reliability of thin film barrier encapsulation. Selecting the appropriate materials and their dimensions will ultimately influence the effect the encapsulation strategy has on the OPV's stability and flexible application. The effect of the combined adhesive and thin film barrier layer on the mechanical robustness and flexibility of encapsulated OPVs is still not fully understood.

Direct deposition:

Thin film encapsulation by direct deposition has been shown to demonstrate excellent barrier properties. [22, 42] While the highly accurate direct deposition technologies such as ALD and CVD eliminate the need for edge seal or barrier adhesive layers, the high temperature and vacuum processing conditions hinder the practicality of commercial adaptation. OPVs and perovskite solar cells (PSCs) are known to be susceptible to thermal degradation. Choi et al investigated the impact of ALD processing temperatures ranging from 95, 105, 120 ˚C on the performance of PSCs. [53] They observed significant degradation at 120 C with the PCE of their devices dropping 35%. There have been several efforts made to develop the deposition technologies to enable open air and low temperature processing conditions. Wang et al. demonstrated a modified plasma enhanced ALD technique, utilizing Al_2O_3 layers coupled with thin aluminum alkoxide layers.[54] The organic-inorganic barrier structure achieved a WVTR as low as 1.3×10^{-5} g m^{-2} d^{-1} and the encapsulated PSCs maintained 96% of their original PCE for > 2000 hours at 30 C and 80% relative humidity. Furthermore, as described in 1.1.3, Channa et al. demonstrated an open-air thin-film deposition technique also compatible with roll-to-roll processing.[45] The fabrication process includes an alternated barrier stack of doctor bladed PHPS and acrylic interlayers which are subjected to a bend to characterize the flexibility and optimal thicknesses of each layer. Figure 10 illustrates the promise of the deposition technique by and encapsulation barrier when compared to a Mitsubishi commercial barrier film and neat PET film.

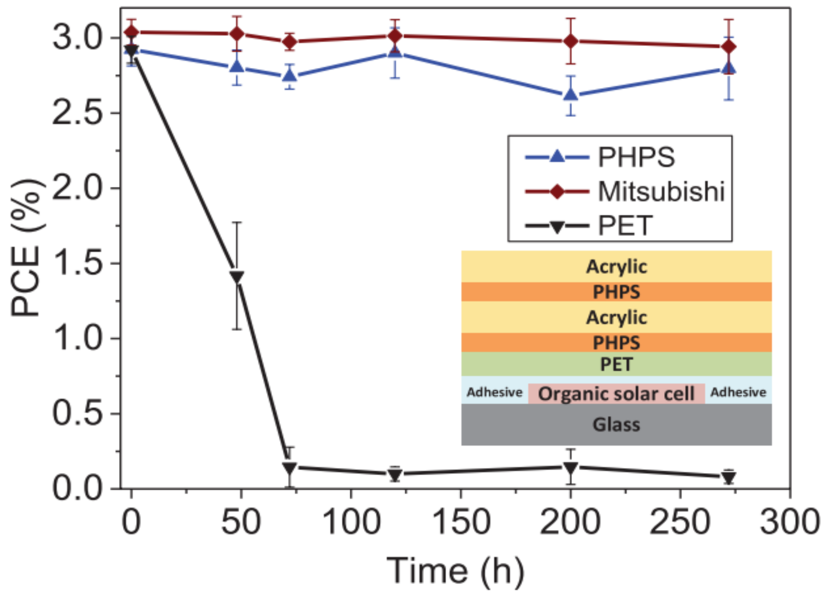

Figure 10. PCE(%) versus Time (h) of multilayer barrier encapsulated OPV. Power conversion efficiency of P3HT:PCBM based OPVs encapsulated with PET foil, commercial Mitsubishi barrier film, or multilayer stack of PHPS and acrylic adhesives over 300 hours under damp heat testing conditions of (40C/85% RH). Adapted from Channa et al *Adv. Energy Mater.* **2019**, *9* (26), 1900598. [(45)]

Further development of direct deposition of thin film barriers is necessary for achieving effective encapsulation of flexible OPVs. Much of the existing technology has been applied to perovskite and organic light emitting diode devices with limited demonstration of OPV applications. Achieving low-temperature, ambient air, and roll-to-roll compatible processing conditions provides an avenue for further investigation. However, consideration of the complexity and cost of the equipment and methodology is of interest as commercial adaptation requires easily scalable processes. Therefore, employing commercially or novel barrier films combined with edge seal or full device area barrier adhesives provides a cost-effective and high throughput flexible encapsulation strategy.

Roll-to-roll encapsulation:

Commercially available flexible OPV devices often employ roll-to-roll (R2R) processing which provides distinct advantages in the fabrication process compared to their rigid and conventional solar counterparts. The method combines the scalable characteristics of OPVs such as low thickness, lightweight, flexible, high throughput processing, and suitability to large-area module production. Demonstrated by many, R2R fabrication involves sequential deposition of the functional layers onto flexible polymer substrates, followed by applying the encapsulation via R2R lamination. Søndergaard et al. thoroughly reviewed the roll-to-roll processing techniques required to achieve the key targets of a minimum of 10% efficiency and 10 years of operational stability.[55] They evaluated the PCE performance of laminated flexible large area OPV devices between flexible polymer barrier films via ultra-violet (UV), hot-melt, and pressure-sensitive (PSA) adhesives. Figure 11 illustrates the three lamination methods and associated stability measurements. It is found that the UV-curable lamination presents the most promising results due to strong edge sealing effect of the thin adhesive layer with minimal bleaching after 900h of constant illumination. Furthermore, the UV-curable adhesive thickness is controllable, allowing for an optimal thickness to be determined. Whereas the PSA and hotmelt methods utilize a predetermined thickness of material, limiting any room for optimization. The PSA method has the fastest processing time being 20-10 m min^{-1} compared to the UV curing and hotmelt method being 2 m min^{-1} and 1 m min^{-1}, respectively. However, to achieve a suitable lifetime using PSAs, two lamination steps are required which produces significant waste as the paper liners must be removed prior to lamination. Therefore, upon evaluation of the stability of the device parameters and lamination, the UV-curable adhesive demonstrates superior performance with R2R processing.

Roll-to-roll processing presents a viable solution for high throughput processing of flexible large area OPV fabrication and encapsulation. The comparison of existing flexible encapsulation strategies is necessary, but existing literature is rather inconsistent in the studies that emphasize device stability. Some record testing under ambient conditions while others test under dry or inert conditions with constant illumination [22]. Establishing a consistent stability testing protocol informed by the International Summit on Organic Photovoltaic Stability (ISOS) should be considered as this will accelerate the understanding of the effectiveness of various flexible encapsulation methods.

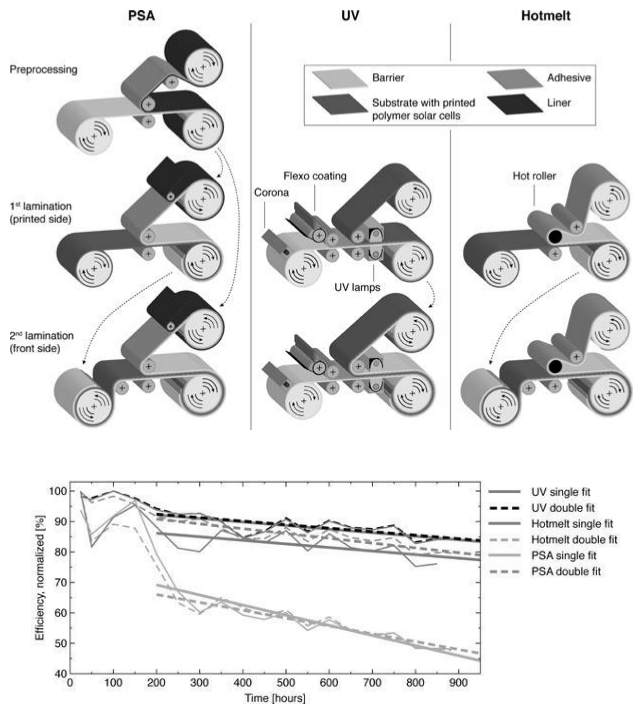

Figure 11. Models of pressure sensitive adhesive, UV curing, and Hotmelt adhesive roll-to-roll encapsulation. The associated efficiencies of P3HT:PCBM devices over 900 hours of constant 1-sun illumination is depicted. Adapted from Hösel et al, *Adv. Eng. Mater.* **2013**, *15* (11), 1068–1075.[55]

1.2 Mechanical Stability of the Encapsulation Layer

1.2.1 Application methods of interfacial adhesives

There are numerous instances of successful demonstration of TFE by lamination, [22, 42] and many of the encapsulation architectures can be categorized by the method of application of the barrier adhesive. The review of emerging TFE architectures conducted by Sutherland et al. and barrier encapsulation method by Weerasinghe et al categorize the most promising structures into complete and partial encapsulation [22, 51]. Complete and partial encapsulation incorporate the use of a barrier adhesive covering the entire OPV area, with the key difference between the two being that a surrounding edge or perimeter adhesive is incorporated in complete architectures, illustrated in Figure 8. While the complete encapsulation architecture has been determined to provide the most effective stability performance,[22, 42, 51] investigating the mechanical reliability of the respective architectures will inform the limitations and potential applications of each.

The lamination process of thin film encapsulation of OPVs is critical to the effectiveness of the established barrier layer. Important parameters to consider are the preprocessing of the barrier materials prior to application, the processing conditions determined by adhesive manufacturers' instructions and sensitivity of the materials used to atmospheric conditions, and the quality of the adhesive layer. The processing conditions and quality of the adhesive layer is dependent on the chemical composition of the barrier adhesive's material. Common full area coverage adhesives generally use transparent epoxies or acrylics or ethylene vinyl acetate (EVA), which is commonly seen in the crystalline silicon photovoltaic industry.[42, 51] Whereas edge/perimeter adhesives may utilize semitransparent epoxies or acrylics as well as elastomers such as polyisobutylene rubber. [22, 42] The mechanical properties of both the adhesive and barrier film should be considered as their toughness and elasticity will influence the response of the encapsulation layer under mechanical stresses.

1.2.2 Encapsulation Failure

The impact of flexible OPV encapsulation and its effect on the extrinsic degradation factors such as irradiation and atmospheric permeation has been thoroughly investigated,[22, 42] but its influence on the mechanical reliability or robustness of the encapsulation has been narrowly defined. In this study, mechanical reliability of the encapsulation should be considered the ability to withstand applied mechanical stress conditions without failure. Failure in most situations can be visually observed by distinguishable wrinkling, cracking, or delamination. Induced fracture or delamination may occur due to loading conditions from applied bending stresses, shrinking and expansive stresses during thermal cycling, and impacting forces from other objects. The combination of tensile, compressive, shear, and torsional stresses as result of these loading conditions may cause failure of the encapsulation layer and thereby lead to accelerated functional loss of the device. The long-term reliability of the encapsulation is also strongly influenced by the adhesive and cohesive properties of the materials used to perform the encapsulation.[18, 28, 56] Daurskardt et al. has demonstrated the importance of interfacial adhesion and integrity by improving the stability of flexible OPVs.[57] The barrier performance of the interfacial adhesives as well as their robustness under mechanical stresses is therefore critical to understand. Thus, the common test methods to evaluate the stability of interfacial adhesives in flexible encapsulation should be defined.

1.2.3 Evaluation Methods

Inconsistent efforts have been made to characterize the mechanical reliability of flexible encapsulation. Seen as a benchmark method of evaluation, monitoring an encapsulated OPV's functional parameters such as the PCE after cyclic bending at a designated bending radius has been demonstrated in a number of instances. [6, 22, 42, 58] However, many other methods of evaluation have been employed such as monitoring the barrier properties of flexible films after cyclic bending or performing basic mechanical tensile tests to identify the mechanical properties such as the Young's modulus or elongation at break. (22, 48, 59) Therefore, evaluating which test methods most accurately inform robust performance is necessary.

Determining the mechanical stability of the encapsulation layer under cyclic bending should be considered as a promising solution. Many have shown that cyclic bending of flexible OPVs can be used to show mechanical stability.(16,58,61) However, introducing an encapsulation layer may impact the flexibility of the overall structure as the flexible device is sandwiched between less flexible adhesive and barrier materials. This loss of flexibility may be minimized by controlling the thickness of encapsulation. The characterization of the stability and assessment of the effectiveness of the encapsulation could be determined by monitoring functional parameters of the device or the barrier performance during testing. However, the encapsulation layer may complicate the ability of the bending test to attribute loss in performance of the functional parameters of the device to failure of the encapsulation layer. However, it should be assumed that the effect of the device stack on the mechanical reliability of the encapsulation can be neglected due to the extremely low thickness of the stack. Therefore, any induced stresses due to bending would be primarily concentrated on the stiffer adhesive and barrier materials of the encapsulation. By assuming processing would be done on the encapsulation layer, application of the bending tests to the evaluation of the mechanical reliability of flexible encapsulation should be considered. Figure 12 illustrates a common bend test and the cyclic bending stability of an unencapsulated device.

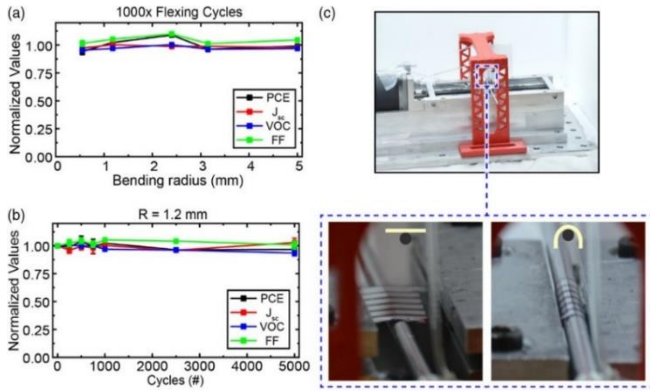

Figure 12. Functional Parameters of an unencapsulated OPV under cyclic bending tests. (a) Plot of normalized functional parameters of a REZEN-based device as a function of radius after 1000 bending cycles. (b) Plot of normalized functional parameters as a function of the number of cycles at a radius of curvature of 1.2 mm. (c) illustration of the designed cyclic bending test apparatus of a sample flat and bent around a rod forcing the uniformity of the bending load. Adapted from Booth et al, *Sol. RRL* **2022**, *6* (9), 2200264. [61]

The radius of curvature of the bend is demonstrative of the robustness and flexibility of the test samples. Describing an encapsulated OPV as "flexible" is often asserted within studies that investigate OPVs fabricated on polymeric substrates.[22] However, interpretation of this description should be clearly defined as the requirements of flexible OPV applications can vary quite dramatically.[11, 17, 22] As described in 1.1.3, the barrier performance can be monitored by a variety of quantitative methods with the Isostatic test method being the commercialized standard. However, this method does not facilitate measurements within the required detectable limits (less than 10^{-6}) that OPV barriers require. Demonstrated by Kempe et al, the Optical Calcium (Ca) Test[52] involves monitoring a freshly deposited calcium pad as it reacts with permeating oxygen and water molecules and can be utilized to achieve adequate WVTR range limits. This method utilizes the unique reaction of the Ca metal reacting with permeated moisture to produce a transparent hydroxide. It is assumed that the reaction is predominantly produced by interaction of the H_2O molecules compared to oxygen. It is controlled by the rate of moisture exposure as demonstrated by Figure 13, thereby facilitating the evaluation of the flexible encapsulation's barrier performance. A quantitative WVTR rate can be determined through this method, however, glass encapsulation is traditionally used as it is impermeable and thereby restricting the permeation to be along the sides/edges. The optical calcium test may be used to evaluate the barrier performance of the interfacial adhesives, however, the effects of the incorporation of a flexible barrier layer should be investigated as the rate of permeation perpendicular to the barrier may be different than along the perimeter of the encapsulation.

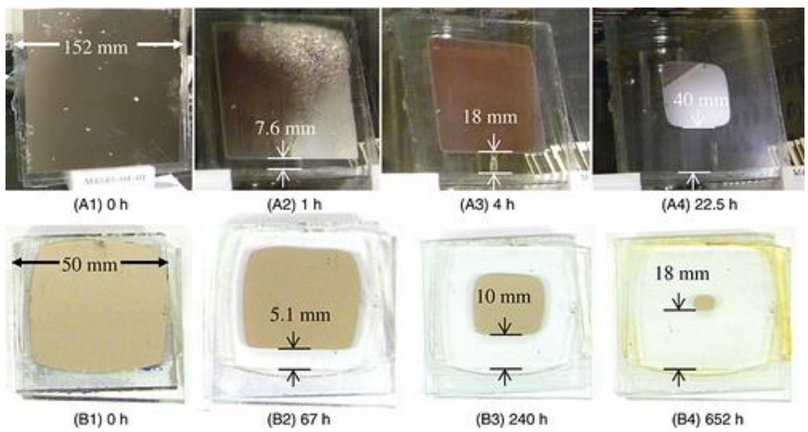

Figure 13. Images of Ca test samples tested at 85 ºC and 85% RH. Calcium metal is deposited onto the blank bottom barrier glass substrate and then covered with an adhesive, followed by a top glass barrier. (A) PDMS between two 152 mm glass samples. (B) Ionomer adhesive between two 50 mm glass samples. Adapted from Kempe et al, *Prog. Photovoltaics Res. Appl.* **2014**, *22* (11), 1159–1171. [52]

The established benchmark bending test provides a comparative method to simulate stress conditions that would be expected for flexible OPV applications. The mechanical stresses associated with bending consider a combination of tensile, shear, compressive, or torsional loads dependent on the loading conditions. These stresses can induce failure of the adhesive or barrier film and present a path of ingress for atmospheric permeation accelerating the loss of performance of the OPV. As OPV device functional parameters are inherently unstable and subject to a variety of degradation factors not specific to bending stresses, distinguishing adhesive failure from other morphological instability after bending can be unclear. To simplify this observation, using the optical calcium test will provide a clear demonstration of barrier failure through visual inspection. Should the adhesive layer or thin film barrier experience failure through cracking, delamination or other failure modes, the calcium pad will provide a quick reaction and allow for simple evaluation of the encapsulation's mechanical stability.

In addition to the bending test and optical calcium test, Juillard et al. demonstrated that the T-peel test (180°) can be used to evaluate the mechanical reliability of flexible encapsulated OPVs by analyzing the mechanical strength and quality of each interface within their devices.(18) The T-Peel test following ASTM D1876 (61), characterizes the peel strength of flexible bonded adherends. The subsequent surfaces after failure were analyzed via IR Spectroscopy and Photoluminescence (PL) to determine the failure type. Analysis of the adhesive strength and common failure modes between the barrier film and adhesive could be considered in evaluating the mechanical reliability of flexible encapsulated OPVs. Investigating the relationship between the adhesive strength and performance of the encapsulation layer under bending may be useful in informing the most appropriate materials for robust performance. Finally, using the T-Peel test to assess the compatibility of the interfacial adhesives with flexible barrier films may reveal optimal surface treatments to enhance adhesion.

1.2.4 Assessing interfacial adhesives in thin film encapsulation

Flexible thin film barriers utilizing the lamination encapsulation strategy demonstrate the most promising solution as the materials are generally low cost and accessible, and the processing is rather straightforward. To understand which test methods most accurately inform mechanical reliability and robustness, this study investigates the performance of interfacial adhesives used in flexible thin film encapsulation under bending and peeling stresses. Full coverage, perimeter sealing, and combined coverage application of the interfacial adhesives will be evaluated for their reliable mechanical stability. Challenges associated with the encapsulation processes reveal the importance of establishing methods that are repeatable and accurate in their assessment of the adhesives. Optimization of the controllable parameters of the encapsulation methods is considered and the influence of the effects of the processing conditions is discussed. Emphasis on the qualitative results determined by the optical calcium bending tests and peeling tests is demonstrated due to limited access to the chemical composition of the sampled adhesives and variability in the mechanical properties provided.

CHAPTER 2: Determining the Mechanical Reliability of Interfacial Adhesives

2.1 Materials and Methods

2.1.1 Materials Used

Mitsubishi Chemical Corporation provided the Mitsubishi VIEWBARRIER flexible thin film barrier. The measured thickness of the thin film was 60 um and consists of an oriented PET film with a sequentially deposited SiO_x layer on top. The reported WVTR of the material is assumed to be > 10^{-4} g m^{-2} day^{-1} based on values observed in the literature.[(45)] The adhesives Photobond LP 4115 and Katiobond LP 655 were provided by DELO Industrie Klebstoffe GmbH & Co. KGaA. The adhesives Eversolar AB-313 and AB-341 were provided by Everlight Chemical Industrial Corporation. The Everlight 341 material is considered reactive due to an integrated getter within the material composition. H.B Fuller provided the Helioseal PVS 101 edge sealant adhesive. The material includes a reactive desiccant within bulk of the material. The EVA-B601 (ethyl vinyl acetate) was provided by Gehring Corporation. Four adhesives were provided and are considered reactive to atmosphere due to the intrinsic properties of the material composition, however due to competing interests the commercial names and provider are undisclosed. Their associated results and sample references will be referred to as SG1, SG2, SG3, and SG4. A summary of the adhesive material types and curing conditions are presented in Table 2 and the material datasheets are provided in the Appendices.

Table 2. Summary of sampled commercial barrier adhesive indicating material type, curing conditions, and suitable encapsulation method.

Commercial Name:	Adhesive Type:	Curing Condition:	Application type:
Delo Photobond LP4115	Acrylic (transparent)	UV irradiation (400 nm > 30s)	Full coverage
Delo Katiobond LP655	Epoxy (transparent)	UV irradiation (400 nm > 30s)	Full coverage
Everlight 313	Epoxy (transparent)	UV irradiation (365 nm > 30s)	Full coverage
Everlight 341	Reactive epoxy (semitransparent)	UV irradiation (365 nm > 30s)	Perimeter coverage
SG 1	Reactive epoxy (semitransparent)	UV irradiation (400 nm for > 30s)	Perimeter coverage
SG 2	Reactive epoxy (semitransparent)	Thermocurable (120C for 30 min)	Perimeter coverage
SG 3	Reactive acrylic (transparent)	UV irradiation (400 nm > 2 min)	Full coverage
SG 4	Reactive acrylic (transparent)	Thermocurable (80C for 30 min)	Full coverage
Helioseal PVS 101	Elastomer w/ desiccant (polyisobutylene rubber)	Thermocurable and applied pressure (110 – 150C)	Perimeter coverage
EVA-B601	Thermoplastic	Thermocurable and applied pressure (140C)	Full coverage

2.1.2 Encapsulation Preparation and Procedure

To facilitate the evaluation of the mechanical reliability of commonly seen flexible thin film encapsulation architectures, the encapsulation of thermally deposited calcium pads is used to model the sensitivity of the materials seen in OPVs. The encapsulation procedure begins with the pretreatment of the materials to remove surface impurities and residual absorbed moisture and air. The commercial barrier thin film is first treated with ultra violet (UV) ozone for 10 minutes and then sonicated in each solution of distilled (DI) water, acetone, and isopropyl alcohol (IPA) for 10 minutes. The samples are then separated into the bottom barrier and top barrier and prepared based on full coverage, perimeter, and combined coverage architectures. The top barriers used for full coverage application are applied with Kapton tape along two of the edges which will provide a spacer during lamination to enable uniform adhesive layer thickness. The top barriers used for perimeter coverage are applied with the hotmelt elastomer adhesive along the edges of the barriers.

Finally, the combined coverage requires an EVA sheet to be placed in the center of the top barrier and surrounded by the hotmelt elastomer to enable complete encapsulation. The flexible encapsulation architectures are illustrated in Figure 14. Subsequently, the barriers and adhesives are stored in a vacuum chamber for degassing for at least 8 hours prior to encapsulation. Due to SG 1-4's and Everlight 341's reactive nature in ambient environments, they are permanently stored in the encapsulation glovebox to prevent compromise of the materials. Following degassing, the materials are transferred to a series of connected gloveboxes for thermal evaporation of the calcium onto the bottom barriers. The encapsulation is performed by spreading the adhesive through roll coating of a glass rod and then application of a flat plate with hand pressure to achieve uniform adhesive dispersion. The curing or bonding conditions vary depending on the adhesive material applied and are summarized in Table 2.

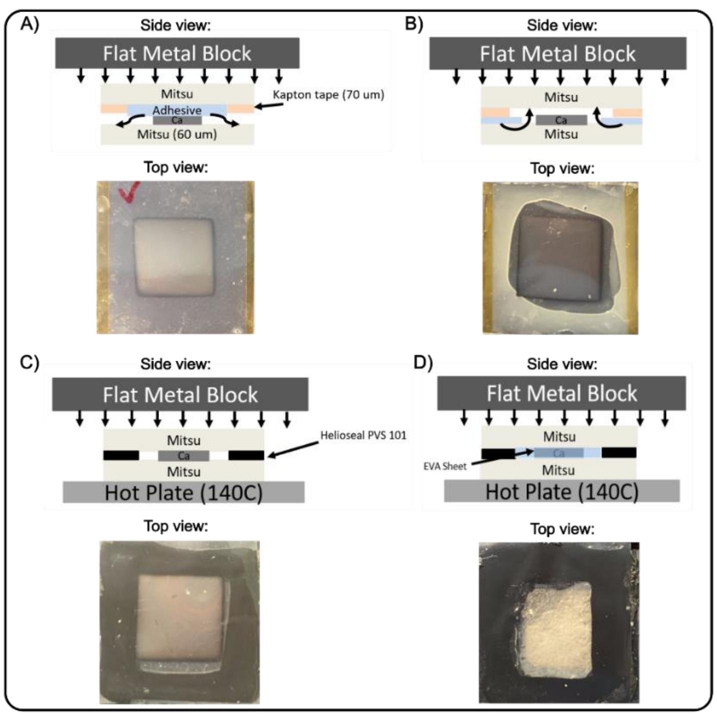

Figure 14. Flexible encapsulation architectures and their processing methods. A) The side and top views of the full coverage encapsulation architecture with transparent adhesive materials, B) perimeter seal with semitransparent adhesives, C) perimeter seal with elastomer adhesive, and D) combined perimeter and full coverage adhesives with elastomer and thermoplastic adhesives.

2.1.3 Peel Test Sample Preparation

In support of the 180˚ Peel test or T-Peel test, adapted by ASTM D1876-08 (2015): *Standard Test Method for Peel Resistance of Adhesives (T-Peel Test),* the following procedure was used to prepare testing specimens. Following the material preparation used for encapsulation, UV Ozone treatment for 10 minutes and sonication in DI water, acetone, and IPA for 10 minutes in each solution was performed on the commercial barrier. The samples were separated into top and bottom films in which on one end of the bottom film, scotch tape was applied to allow for an unbonded grip area. The adhesives were applied and bonded in the same manner as described in 2.1.2. All materials except Everlight PB 341 and SG 1-4 were bonded in ambient lab conditions for ease of processing. The bonded samples are then laser cut using a CO2 laser, Universal VLS6.60, to establish uniform dimensions and to minimize inducing stresses from cutting that may alter the adhesion strength of the bonds. Final sample thicknesses ranged from approximately 60 μm to 660 μm dependent on the barrier adhesive material applied.

2.1.4 Combined Bending and Optical Calcium Test

Simulating realistic the stress conditions that flexible encapsulated OPV applications must endure can be achieved through bending of the encapsulated structure. As described in 1.2.1 there are several methods of applying the bending load to the structures. This investigation utilizes a bending stage rotated by a connected servo motor, controlled by an Arduino code.The design incorporates adjustable control of a testing specimen's position and bending radius. However, shown in Chapter 3, some encapsulated calcium samples demonstrate adhesive failure at bending radii larger than what is sufficiently supported by the stage. To facilitate the evaluation of the mechanical reliability of the flexible TFE architectures, manual bending is performed across circular objects ranging from 2.5 mm to 17 mm bending radii. Encapsulated samples first undergo the manual bending test to identify the bending limit of the adhesive materials and encapsulation strategies. The bending limit is established by visually inspecting a freshly encapsulated sample and then upon one bending cycle across an object, the sample is inspected for cracks, delamination, or other signs of barrier failure. Images are taken periodically after failure has been identified to demonstrate the critical functionality of the barrier in its prevention of permeated moisture. Figure 15 illustrates various performed bending tests.

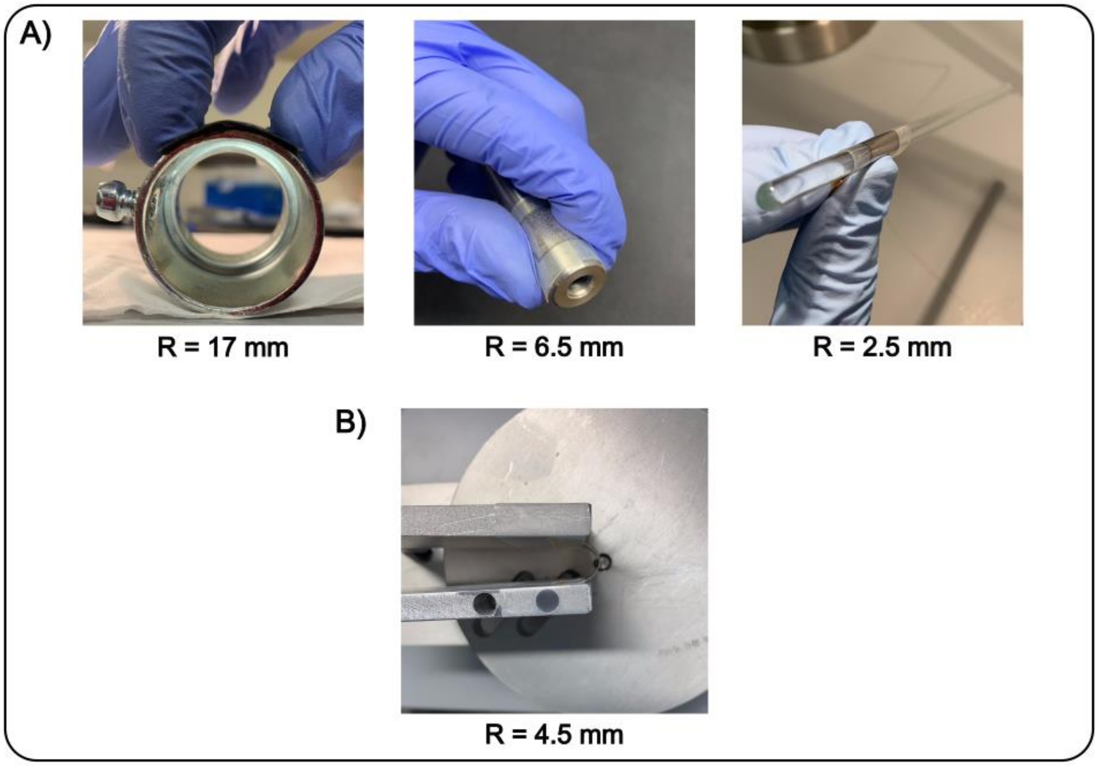

Figure 15. Manual and cyclic bending tests. A) Various manual bending tests that are performed across applying the encapsulated calcium samples across circular objects with defined a radius of curvature. B) Image of sample in the rotating bending stage at the maximum distance from the neutral axis. Radius is defined as half the distance between the plates when parallel.

Once the bending limit is established, the barriers compatible with the mentioned bending stage are subjected to cyclic testing to investigate the performance under repetitive loading. The rotating bending stage is performed on samples with bending limits below 7 mm radius of curvature. Clamping or adherence of the test samples to the rotating stage is performed by applying scotch tape. The following parameters are predetermined to establish consistent testing conditions and methods: distance of rotation (0-360˚), the rate of bending (rad/s), and the number of cycles. Thin film encapsulated OPVs have demonstrated stability under cyclic loading, but characterization of the performance limit and mechanical reliability of the common TFE strategies have yet to be extensively explored. The combined bending and optical calcium test demonstrate a unique method of informing the robustness and reliability of TFE architectures.

2.1.5 Peel Tests

Application of the T-Peel or 180˚ Peeling test to assess the mechanical reliability of the flexible encapsulation layer has revealed that the adhesive and cohesive properties of the bonding layer significantly influence its resilience to applied stresses. Thus, informed by ASTM D1876, the T-Peel test is performed on prepared samples by the delaminator machine. Prior to conducting the tests, each sample's total thickness, adhesive layer thickness, and specimen width is noted. Subsequently, the peeling rate is specified at 5 mm/min along with the total displacement distance. The delaminator records the loading force over the total displacement distance and the typical behavior of the graph can be characterized by Figure 16. The linear portion of the graph denotes the loading required to initiate the peel or failure of the bond followed by a sharp drop into a plateau or constant peeling behavior. The peel strength, recorded as N/mm, is the average load per unit width of the bond line required to separate the adhered materials and the angle of separation of 180 degrees. The average is found by considering the most stable portion of load displacement graph and taking the average of the load values across this section and dividing it by specimen's width. In situations where the behavior of the graph does not follow Figure 16, this can be understood by the characterization of the quality of the adhesive layer and the observed failure mode. The thickness of the adhesive layer, pretreatment of the materials, and sample specimen dimensions influence the observed behavior of the graph. Optimization of these parameters shall be considered as their influence on the adhesive strength of the material may inform design and processing conditions that yield enhanced mechanical reliability.

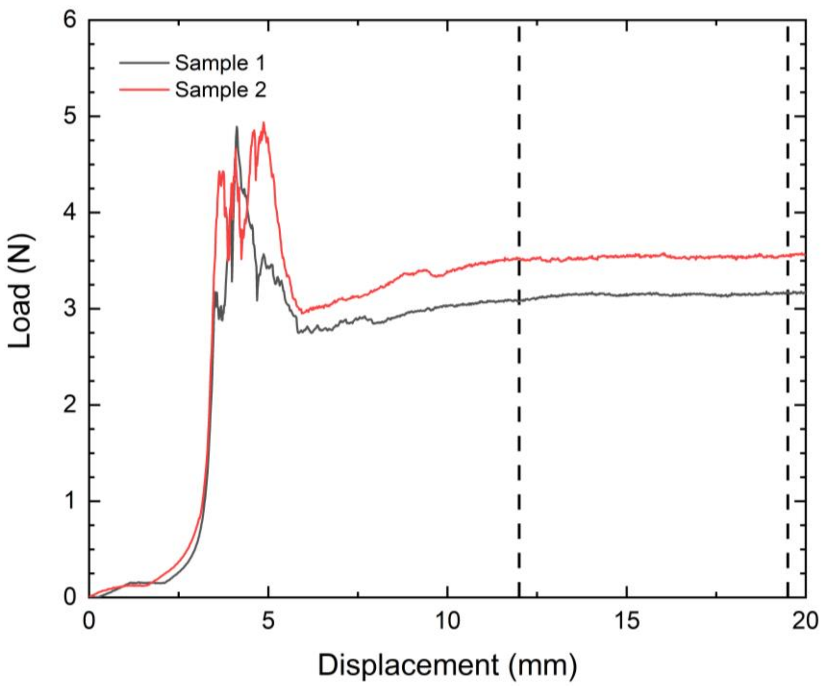

Figure 16. Plot of normal load versus displacement graph of T-Peel Tests. Plot resembles proper curing, uniform adhesive thickness, proper alignment of peeling arm, and similar peel arm geometry. Peel strength (N/mm) is calculated between the most consistent measured load.

CHAPTER 3: Assessment of the Interfacial Adhesives

3.1 Encapsulation and Testing Challenges

3.1.1 Optimization of Encapsulation Architectures and Processes:

Applying the encapsulation layer often caused the presence of defects such as bubbling, pinholes, smearing, or adhesive overflow to arise within the adhesive layer. The optimization of the application of the adhesive layer would improve the accuracy and overall consistency of the observed behaviors for each encapsulation method. Figure 17 illustrates the visible bubbling and pinholes defects. The bubbling can be contributed to the application of the adhesive in which an applicator tool was pushed up and down in a dabbing motion to transport the adhesives from their storage vials to the substrate. This created residual bubbling in the adhesive layer that was not dissipated by the bar roll coating or applied pressure of the flat plate during encapsulation. The pinholes are attributed to the residual gas or air bubbles that formulate during the final curing process of the adhesives. The release of the tiny air molecules that were absorbed by the adhesive during storage in atmosphere gave rise to large amounts of pinholes. To mitigate this effect, prolonged degassing conditions or permanent storage in the inert atmosphere of the glovebox should be considered.

The average bond thickness of each sample was also determined and shown in Figure 17. The thicknesses were found by measuring the total thickness of the laminated samples with dial calipers and then neglecting the combined thickness (120 um) of the top and bottom barrier film. The reactive acrylic material applied in the full coverage encapsulation method was the only material that yielded consistent adhesive layer thicknesses. The Kapton tape applied to the edges of the top barrier film served as a spacer and was determined to be 70 um which was the effective average thickness of the reactive acrylics. However, the other materials employed varied significantly in their total bond thicknesses, demonstrating the inconsistent functionality of the Kapton tape. Adhesive over flow seen in Fig 17B) often occurred due to excess application of adhesive material. Therefore, when the top barrier film was applied excess adhesive would overflow outside of the stack, effecting the stiffness and overall thickness of each sample. A controlled measurable dispensing method of the adhesive combined with an evenly applied pressure for complete dispersion would improve the quality of the layer and mitigate any excess material flow out of the encapsulated structure.

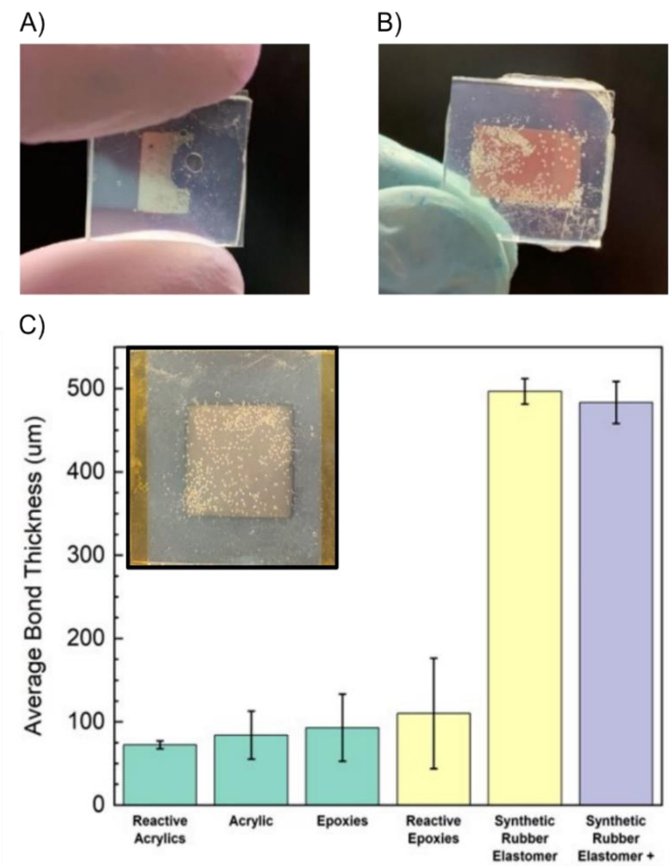

Figure 17. Defects present in encapsulated samples. A) Presence of air bubble defect affecting rate of permeation reaction B) Pinholes defects and adhesive overflow after curing C) Average bond thickness vs. adhesive types with standard deviation of averages depicted. Inset) demonstrates pinhole presence regardless of Kapton tape spacer application (yellow strips).

The combined coverage and perimeter sealant materials were significantly greater in bond thickness due to the limited surface area to be able to compress on. The elastomer and thermoplastic adhesive require significant pressure and adequate space to compress under to achieve thicknesses in the same magnitude of the barrier film (<100 μm). The adhesive layer thickness has been shown to affect the strength of the adhesive bond. [65, 66, 67] However, the layer thickness would likely need to be less than 100 um, as evidenced by the observed results, to achieve mechanical reliability in robust flexible applications. Identification of the optimal adhesive layer thickness that provides sufficient barrier performance and mechanical reliability should be considered. This could be concluded by performing an iterative analysis on the permeability and reliability performance of varied bond thicknesses of each encapsulation method. However, achieving uniform defect free adhesive layers is required to ascertain an accurate assessment. Finally, considering the ideal specimen dimensions to allow for appropriate compression of the elastomer and thermoplastic materials may yield lower average bond thicknesses and affect the observed mechanical reliability of the adhesives.

3.1.2 Reliability of the combined optical and bending tests:

Prior to the introduction of combining the optical calcium test and bending test, each test has been shown to evaluate the stability of the parameters critical to the commercialization of flexible OPVs. Kempe et al. demonstrated the effectiveness of the optical calcium test at evaluating the barrier performance of edge sealing adhesives.[52] Others performed the bending tests on OPVs and monitored the stability of the PCE and functional parameters (JV, VOC, FF, etc.) after cyclic bending.[58, 68] Additionally, the bending test has been used to demonstrate the stability of the barrier performance of nanocomposite and other promising encapsulation barrier films.[22, 47] Combining the optical calcium test with the bending tests introduces a reliable and efficient method of evaluating the mechanical reliability of flexible encapsulation architectures. Figure 18 illustrates the time lapse of two samples that were used in the manual and cyclic bending tests. Encapsulated calcium samples without induced failures have been demonstrated to show prolonged stability due to the effects of the adhesive and barrier film layer.[52] The images shown in Figure 18 evidence the ability of the combined tests in providing a simple but effective method of evaluating the mechanical reliability of flexible encapsulation architectures.

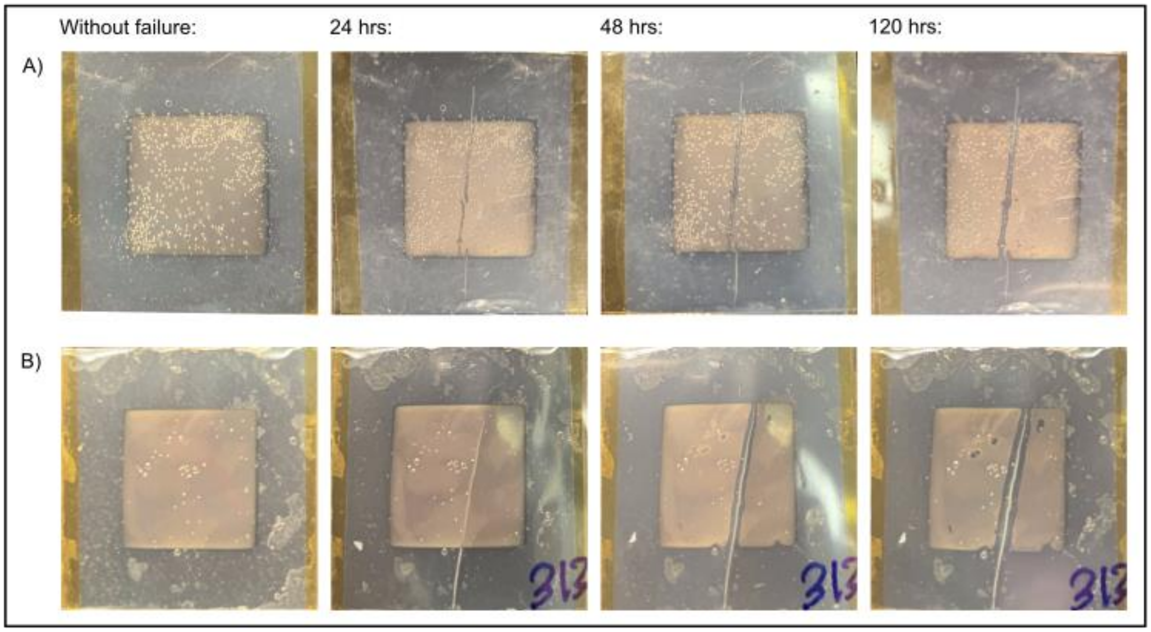

Figure 18. Reliability of optical calcium bend tests. A) Time lapse of the reaction of the 300 nm calcium pad after the Delo Katiobond LP 655 full coverage epoxy adhesive experienced a cracking failure during the manual bending limit test. B) Time lapse of the same reaction but with the Everlight 313 full coverage adhesive experienced failure during the cyclic tests.

The time lapse highlights the effects of the presence of defects and failure in the adhesive layer on the stability of the calcium. The stress and strain conditions applied to the samples under bending are affected by the bending rate and clamping conditions described in 2.1.4. Fatigue failure conditions may be considered under the cyclic bending test as samples were not able to withstand significant amounts of repeated loads without failure. Investigation of the failure modes and how they are influenced by the strain rate, number of cycles, and loading conditions is necessary to inform the mechanical reliability of common TFE architectures. Furthermore, the clamping or adherence of the samples to the bending stage could be improved. Seen in Figure 19, applying scotch tape to adhere the samples to the bending stage allowed for small movement around the clamped edges. This may have impacted the uniformity of the bending radius and applied stress on each sample. Furthermore, reliable processing and encapsulation methods are of upmost importance to improve the consistency of the samples. Extensive studies have been performed on thin film polymers regarding their failure mechanics, [57,69,70] however investigation into the mechanical behavior of thin film adhesives confined by flexible adherents has been narrowly defined.[71] Combining the optical calcium test with the bending tests establishes a method to reliability assess the mechanical stability of interfacial adhesives in robust bending conditions.

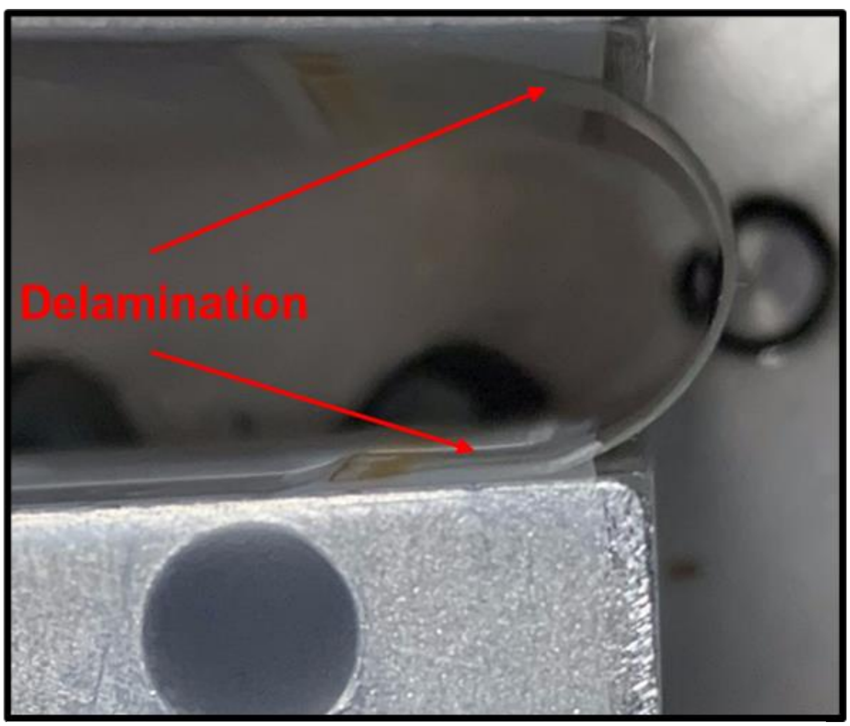

Figure 19. Delamination at the edges of adhered samples during a cyclic bending test.

3.2 Robustness of the flexible encapsulation architectures

3.2.1 Mechanical Stability under Bending Stress

In this section, the analysis of the results after bending thin film barrier encapsulation architectures is discussed. The observed bending limit of each encapsulation architecture informs the mechanical stability of each architecture type and evaluates the effectiveness of the combined optical calcium bending test at establishing mechanically robust encapsulation. As described in Chapter 2, ten total encapsulation architectures were subjected to the manual bending test to establish the bending limit of the materials and characterize the mechanical reliability of each method. The following results have been organized by their encapsulation method: full area, edge or perimeter sealing, and combined coverage. The sampled adhesives were grouped by the material type and their respective bending limits characterize the range of each encapsulation method. The failure modes that inform and characterize the bending limits are described in Figure 20.

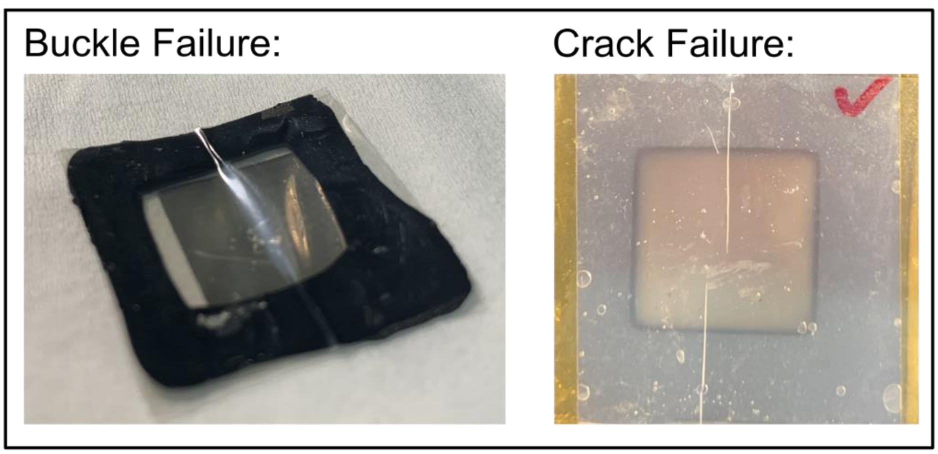

Figure 20. Buckle failure and crack failure of interfacial adhesive encapsulation methods.

The manual and cyclic bending test results were concluded when buckling or cracking was observed. The encapsulation architectures utilizing the elastomeric perimeter sealing adhesives demonstrated buckle failures. This was driven by the concentration of compressive stresses along at the edges of the delamination of adhesive and barrier film thereby buckling the unadhered portion of the barrier film. The buckle failure typically occurred along the middle of the sample or the maximum out of plane displacement location of the barrier film. This is because of the poor adhesion and incompatibility of the thicker elastomer when used with the much thinner barrier film (~600 μm vs. 60 μm). Adhesive materials that comprised of epoxies and acrylics, regardless of their reactive properties, experienced cracking failure. This was due to a critical stress intensity located at defects within the adhesive layer and therefore initiating the propagation of the strain energy release. By grouping the adhesive materials by their encapsulation method and understanding the stress conditions that induced failure, the range of reliable mechanical stability is depicted in Figure 21.

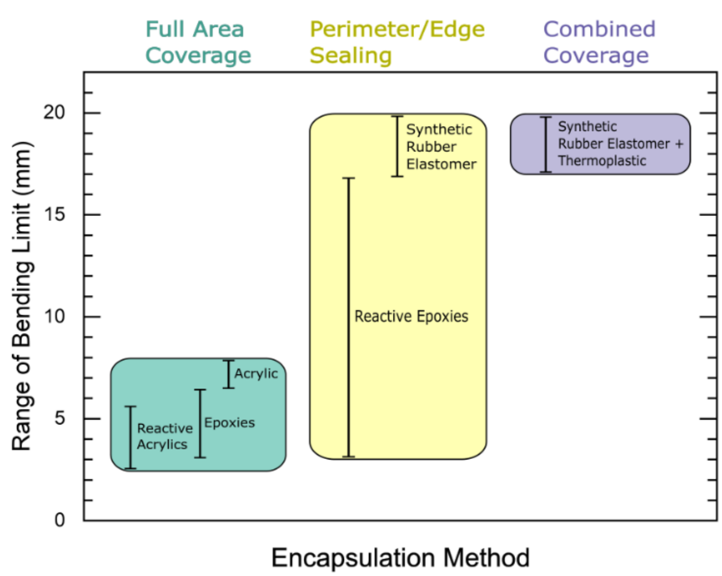

Figure 21. Range of bending limits of full area coverage, perimeter/edge sealing, and combined coverage flexible encapsulation methods. The samples materials characterize the range of bending limits of each method with the reactive acrylics showing the lowest range and the rubber elastomer in the largest range.

The range of the bending limits of each encapsulation method are found to be **2.5 – 8 mm, 3 – 20 mm, and 17 – 20 mm** for full area, perimeter, and combined coverage, respectively. The range of the bending limits suggests that the full area coverage encapsulation method demonstrates the most reliable mechanical stability with consistent bending failure below 8 mm. While the perimeter/edge sealing method suggests the possibility of achieving effective mechanical reliability, the variability of the data shows inconsistent robustness and therefore the full area coverage method should be considered for further evaluation. To further evaluate the mechanical stability of the full coverage interfacial adhesives, the cyclic bending test was performed. The adhesives tested under cyclic conditions were selected based off their bending limit. A cutoff of mechanical stability under 8 mm was selected as it captured all of the adhesives that withstood the manual bending test without failure above the 6.5 mm object radius. The results from the cyclic bending test are summarized in Table 3.

Table 3. Summary of the average number of cycles until failure at 1 mm above the lowest observed bending limit of each material. (*) Two Everlight PB 313 samples withstood > 150 bending cycles at 6.5mm and only failed when lowering the testing radius to 5.5 mm.

Commercial Name	Material Type	Average Thickness of Adhesive (um)	Radius of Curvature Tested (mm)	Average # of cycles until failure
SG 1	Reactive Epoxy	70	6.5	5
SG 2	Reactive Epoxy	50 ± 28	4.5	10
Delo Katiobond LP 655	Epoxy	80 ± 17	5.5	2 ± 2
Everlight PB 313 (*)	Epoxy	80 ± 14	5.5	30 ± 7
Delo Photobond LP 4115	Acrylic	72 ± 13	6.5	4 ± 8
SG 3	Reactive Acrylic	70	4.5	40 ± 50
SG 4	Reactive Acrylic	70	4.5	12 ± 10

The findings from the cyclic bending test highlighted the effects of the variability in the adhesive layer's uniformity described in 3.1, which was seen to affect the majority of tested samples. Additionally, the majority of the adhesives tested were not able to endure repeated bending stresses without failure. However, the epoxy and reactive acrylic material types demonstrate capability to endure cyclic loading. In fact, the Everlight PB 313 material endured 150 cycles at 6.5 mm and only failed when lowering the bending radius to 5.5 mm. This may be attributed to the uniformity of the adhesive layer with minimal defects present. Furthermore, the variability of the results reiterates the effects of the presence of defects and variable bond thicknesses. The selection of the tested bending radius was decided by choosing a bending radius 1 mm above the average manual bending limit of each sampled material. This was done to understand the reliability of the barrier layer when repetitive loading is induced sufficiently above the average failure bending limit. While the variability in the data limits the analysis of the induced stress conditions resulting in the failure of the encapsulation of each sample, a general application of laminated thin film mechanics can be applied to understand the observations.

3.2.2 Analyzing the Failure Modes

Laminated structures involve use of elastic materials with variable thicknesses and mechanical properties, and it is expected that the stresses experienced during bending will consist of a combination of tensile and compressive forces. As the degree of curvature or the radius decreases in size, both the loading is increased and the bending energy increases with the out of plane displacement.[(61)] Combining this with a mismatch in the elastic modulus between the adhesive layer and thin film barrier results in a compounded loading conditions sufficient to initiate failure.[(62, 63)] The common failure types experienced by thin film multilayer structures is delamination/debonding at the interface or cracking of the adhesive layer. These are driven by the in plane tensile and compressive forces and ratio of the toughness of the layer and bonding interface.[63] When the stress is predominantly compressive, buckling induced interface delamination is observed. Cracks are often initiated at a localized stress point such as a defect within the bulk of the adhesive layer and upon loading, the crack may propagate at critical stress or energy density explained by linear elastic fracture mechanics (LEFM).[64] The plastic deformation surrounding the crack tip region and compressive normal stresses at the crack tip drive the propagation of the cracks when subjected to cyclic loading conditions. The mismatch in mechanical properties between the adhesive layer and barrier film challenges the characterization of the predicted bending behavior. However, it can be assumed that the flexibility and low thickness of the Mitsubishi film concentrates the stress distribution to the stiffer adhesive layer.

The adhesive layer thickness and its effect on the overall stiffness of the encapsulated structure cannot be neglected. Wyser et al. developed a model for predicting the bending stiffness of multilayer laminates with thin adhesive layers.[65] The findings suggest the bending stiffness is influenced by the thickness and elastic modulus of the adhesive, however predominantly controlled by the thickness and location of the adhesive layer. The thickness range considered in this investigation is magnitudes larger due to the design of the system and requirement of suitable barrier properties. However, the mechanical reliability of encapsulated structures must consider the robustness of the adhesive layer and its behavior under single and cycled loading conditions at varied thicknesses. Adhesive plasticity will contribute to the nonlinearly of the stress distribution, therefore further understanding of the viscoelastic behavior at varied loading conditions may inform the limitations of the adhesives sampled. However, due to the limited knowledge of the mechanical and chemical composition of the adhesives sampled, investigation of the influence of the mechanical properties on the bending behavior could not be considered.

The observations from the bending performances of the flexible encapsulation architectures using interfacial adhesives provides a reliable testing method to evaluate the robustness of flexible thin film encapsulation. The full coverage encapsulation architecture was shown to consistently achieve reliable robust performance. The application of interfacial adhesives across the entire surface area of the substrate should be considered for mechanical reliability. Perimeter sealant adhesives of the elastomeric material type should be limited to applications that do not require significant flexibility due to the poor adhesion with flexible adherents. While the reactive epoxies within the perimeter sealant adhesive application demonstrated significant robustness, the range of bending performance would require further testing to make a more conclusive observation. Furthermore, the selection of the barrier film and adhesive used should consider the mechanical properties as flexible performance and reliability is driven by the coupling of the materials.

3.2.3 T-Peel Test Failure Modes

T-peel tests failure mechanisms range from adhesive/interfacial failure, cohesive failure, and mixed failure. Each of these failures were observed during testing and were observed to influence the average peel strength across each material and are illustrated in Figure 22. The parameters of the T-peel system that are understood to affect the results are the bending geometry during peeling, specimen dimensions, and thickness of adhesive layer.[72, 73] The bending geometry of each "arm" of the T-peel test is dependent on the elasticity of the material. The Mitsubishi commercial barrier film was used for both the top and bottom layers of each specimen, which is understood to transfer the stress concentration to the adhesive bond. The specimen dimensions were held consistent across samples therefore comparison of the mechanical reliability of the materials used in TFE could be conducted.

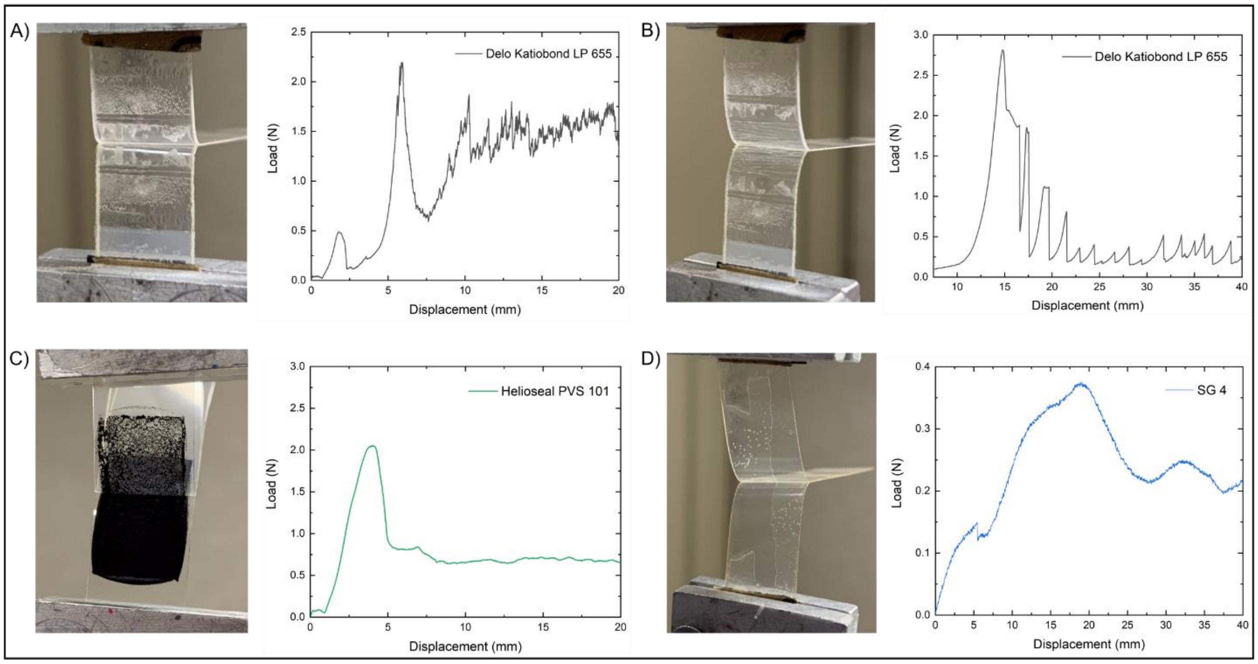

Figure 22. Cohesive, Stick-Slip, and Interfacial failure modes from T-Peel Tests. A) Illustration of cohesive failure experienced by the Delo Katiobond LP 655 adhesive and associated load versus displacement graph used in finding the peel strength (N/mm). B) Stick slip failure behavior experienced by the Delo Katiobond adhesive. Small brittle cracks can be seen which characterize the sharp jaw tooth pattern. C) Traditional interfacial failure experienced by the Helioseal PVS 101 adhesive which is demonstrative of a linear peak until peel propagation is held constant. Residual adhesive is seen remaining on the other bond arm demonstrative of minor mixed failure. D) Varied interfacial failure mode of the SG 4 adhesive which demonstrates inconsistent behavior in the plot.

By considering the peel tests as fracture tests, the fracture characterization can be separated into initiation and propagation. The force versus displacement graphs displays the variety of failure modes that can occur. The initial peak of the graphs can be attributed to the load required to initiate the cracking of the bond. The crack initiation load may be influenced by misaligned specimens, adhesive overflow, defects near the crack tip, insufficient clamping force, or plasticity of the adherends.[73] The larger peel strengths were observed to be the result of cohesive failure (Fig. 4A). This is due to the higher fracture energy required to initiate interfacial rupture determined by stronger intrinsic adhesion forces acting at the interface. Therefore, more strain energy and a higher load is needed to break the interfacial atomic and molecular bonds causing the rupture to localize within the bulk of the adhesive. Stick slip behavior is commonly observed in peel tests (Fig. 4B) where the cause is associated with crack tip blunting in viscoelastic systems (stick) and followed by an initiation force where a sudden crack (slip) advances in a brittle manner.[73] Reasoning for the observed behavior may be explained by local defects within the adhesive materials, variations in the locus of failure (cohesive, interfacial, and mixed), evolving specimen compliance, rate-dependence, and other reasons outside the scope of this investigation .[73,75,76] Figure 4C shows the common interfacial failure mode where an initial peak is observed followed by a plateau and subsequent steady state peeling. This can be understood by the strain energy dissipated to the interface being greater than the work of adhesion (W_{adh}) being thereby initiating rupture of the interfacial bonds.[77] Finally, the uneven interfacial failure seen in Fig. 4D can be attributed to the defects present at the crack tip and within the adhesive layer combined with misaligned peeling arms. The bending geometry and associated peeling strength are strongly correlated with the alignment of the peeling arms which influences the uniformity of the applied load on the adhesive layer.

3.2.4 Mechanical Stability under Peeling Forces

The materials used are categorized by their encapsulation method and the average peel strength (N/mm) of each material is compared. Figure 23 shows the observed results of the peel tests. The Delo Katiobond LP655 (epoxy), Photobond LP4115 (acrylic), and material SG2 (reactive epoxy) demonstrate the highest observed peel strengths. However, the Everlight PB 313 (epoxy), SG1 (reactive epoxy), SG3 & 4 (reactive acrylics), which showed mechanical reliability under robust bending conditions, had dramatically different average peel strength. The variability in the data can be explained similarly by the presence of defects and non-uniform layer thickness as described in the encapsulation/lamination process.

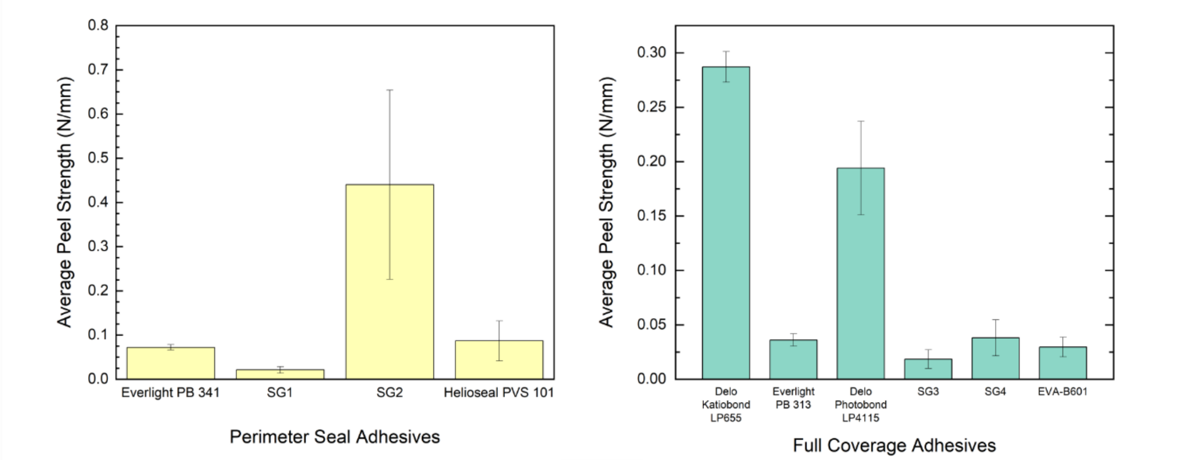

Figure 23. Plots of the average peel strength (N/mm) and standard deviation. Materials which are categorized by their encapsulation method.

The behavior of the peel and measured load was observed to be directly associated with the type of failure experienced by the bond. Samples that experienced cohesive bond failure resulted in the greater average peel strengths demonstrated by the Delo adhesives and SG2. Samples that experienced interfacial failure or stick slip debonding had much lower peel strengths. All of the adhesives were applied across the total area of the test specimens except for the gripping area. The average adhesive thickness was 86 ± 43 µm for the epoxy and acrylic materials, and the perimeter sealing EVA-8601 and Helioseal PVS 101 were 425 ± 25 µm and 618 ± 40 µm, respectively. It is known that thickness of the adhesive layer has an effect on the observed peeling strength.[72] The shear strength of adhesive joints has also been suggested to demonstrate a thickness dependence. [66, 74] While there is thickness variability across the material categories, the specific thickness dependence on for each material was not investigated for its effect on the peel strength. While the failure modes are driven by the thickness dependence of each material, observing the peel strength under the framework of fracture reveals the basis of the behavior of each failure type.

Table 4. Average Peel Strength, Lowest observed bending radius (mm), and Average bending cycles (# cycles) of the epoxy and acrylic adhesives.

Adhesive Name	Average Peel Strength (N/mm)	Lowest observed bending radius (mm)	Average bending cycles (# cycles)
Everlight PB 313 (epoxy)	0.036 ± 0.0056	5.5	30 ± 7
Delo Katiobond LP 655 (epoxy)	0.287 ± 0.014	5.5	2 ± 2
SG 2 (reactive epoxy)	0.44 ± 0.214	3	10
SG 3 (reactive acrylic)	0.038 ± 0.0165	2.5	40 ± 50
SG 4 (reactive acrylic)	0.0184 ± 0.0085	4	12 ± 10

Correlation between the peel strengths and bending performance of the interfacial adhesives was not demonstrated as shown in Table 4. The application method of the interfacial adhesives also did not establish a trend in the average peel strengths. This was concluded as the perimeter and full coverage encapsulation methods both showed adhesives with high peel strengths. Therefore, the T-Peel tests results should be considered as an informative test method to evaluate the compatibility of interfacial adhesives with flexible substrates. The ability for adhesives to establish stronger bonds than others may be informed by the surface characteristics of the adherend. Influence of the surface tension and energy on the wettability of the interfacial adhesives was not considered but should be investigated.

Applying limited fracture theory to the observed results emphasizes the importance of the testing conditions and parameters of the delaminating device and the samples. The mechanical reliability of the adhesive materials commonly seen in thin film encapsulation can be evaluated by the T-Peel tests however a strong correlation between the bending reliability and peeling force was not observed. The materials sampled demonstrate significant variability in their peeling strengths likely due to defects within the bulk of the adhesive and at the crack tip. The thickness dependence and its influence on the observed failure modes was not fully considered but may reveal design considerations that impact the mechanical reliability of the interfacial adhesives in flexible encapsulation.

Conclusion

This investigation was concerned with determining which flexible encapsulation architectures and processing methods result in mechanically robust or reliable organic photovoltaics. Evaluating the mechanical reliability of common flexible thin film encapsulation systems and processes would be informed by established test methods seen in literature. A series of mechanical bending and peeling tests were conducted to consider the effectiveness of each method in informing the mechanical stability of the encapsulation methods. It was determined that the encapsulation architectures that demonstrated the most consistent stability were the structures that utilized full area coverage/application of an epoxy or acrylic adhesives between two thin film commercial barrier layers. The failure modes that informed the evaluation of each encapsulation architectures were categorized by wrinkling of the barrier layer or cracking of the adhesive layer. Wrinkling failure is observed by delamination and induced buckling of the barrier layer due to the poor interface adhesion of elastomer and thermoplastic materials under tensile stresses. Cracking failure was attributed to the induced concentrated strain energy at the defects of the adhesive layer during bending and therefore propagation of the crack at a critical loading stress.

By combining the bending test with the optical calcium test, a reliable method of evaluating the mechanical stability of flexible encapsulation systems was established. By using calcium as the moisture sensitive measurement, tedious time and costs associated with the fabrication and testing of flexible encapsulated OPVs was mitigated. However, the impact on the mechanical reliability when translating the encapsulation to flexible OPVs should be considered. Furthermore, the barrier performance of the adhesive barrier material could be evaluated qualitatively as the rate of oxidation of the calcium surrounding the observed failure could be measured.

The T-Peel tests demonstrated how the quality and uniformity of the barrier adhesive layer can affect the observed results. Barrier adhesive materials showing mechanical resilience under the bending tests did not translate to having the highest peeling strengths. However, the T-Peel test can be used to analyze the fracture energy of the adhesive materials to inform proper material selection for flexible encapsulation. Further analysis into the observed failure modes of adhesive bonds is required to understand how the T-Peel tests accurately inform the mechanical stability of flexible encapsulation architecture. It is clear that the optimization of the encapsulation or lamination process significantly impacts the observed results.

The test method that most accurately informs the mechanical reliability of thin film flexible encapsulation is the bending test. The epoxy and acrylic interfacial adhesives applied in full coverage encapsulation were the best performing materials under the bending and peeling tests. Additionally, the mechanical properties of both the barrier and interfacial adhesives should be considered in selecting the most appropriate combination for flexible thin film encapsulation.

CHAPTER 4: Future Work and Considerations

4.3 Achieving Uniform Encapsulation and Enhancing Adhesion

Determining the encapsulation architectures and processing methods that result in mechanically robust flexible OPVs was established through this investigation. The introduction of a reliable method of evaluating the mechanical stability of interfacial adhesives using flexible thin encapsulation was also described. However, the variability of the results shown in both the manual and cyclic bending tests as well as the T-Peel tests necessitates a more optimized encapsulation process. The accuracy of findings from the bend and peel tests will inform the design of the encapsulation architecture and selection of the appropriately suited materials. Establishing a more effective encapsulation method that is less variable and dependent on the user's controlled application of the adhesives and materials will ultimately improve the consistency and quality of the encapsulation layer. Two methods that may address this issue are the incorporation of syringe fluid dispensing equipment that is compatible with high viscosity adhesives or considering gravure roll coating.

Syring fluid dispensing equipment compatible with high viscosity adhesives would be relevant to consider in the application of the epoxy and acrylic adhesives used in this investigation. Not only would this equipment allow for the capability of a quantifiable amount of adhesive to be applied, but the application process would be able to be controlled through the use of a pressurized dispensing mechanism. By incorporating a pressurized dispensing method, the air bubbles present during the current application method would be mitigated as the up and down motion of the applicator tool in the storage vial of the adhesive often created unwanted residual air bubbles after application. However, this method would still require the application of a blade coating or bar coating process to allow for even dispersion of the adhesive across the sample.

Gravure roll coating would provide a suitable solution to this challenge as the process utilizes an engraved roll (gravure or applicator roll) to apply a premeasured amount of adhesive, followed by a doctor blade to wipe off any excess. The film would be sandwiched between the engraved roll and a rubber backing roll to achieve uniformly applied layers of adhesive. This method is demonstrated in the roll-to-roll encapsulation section in 1.1.4 and should be considered as an optimal method to achieve defect free adhesive layers with uniform thickness. The current method of application often causes excess adhesive to remain after application of the top layer. This created non uniform bending behavior or uneven peeling conditions which affected the accuracy of the results of the bending and peeling tests. Enabling gravure coating capability would alleviate this issue and enhance the ability of the bending tests to inform mechanically robust performance of the interfacial adhesives.

Optimized encapsulation methods would improve the uniformity of the adhesive layer, but various preprocessing conditions should be considered such as the storage conditions of the adhesives or the treatment of the substrates prior to encapsulation. Proper storage conditions of the materials may impact the frequency of pinhole defects within the adhesive layer as residual gas molecules were released during curing. Two solutions are increasing the duration of the degassing process to mitigate the presence of pinhole defects or permanent storage of the adhesives within inert environments to eliminate uptake of moisture or oxygen molecules.

Additional surface treatments to enhance the ability of the adhesives and barrier materials to achieve stronger adhesion may be addressed through the pretreatment of the barrier films. Treatments such as inducing roughness or functionalization through plasma ozone treatments may enhance the adhesion strength and improve the reliability of the bond.[78, 79] By inducing roughness to the surface, additional bonding area is enabled for the adhesive to adhere to as well as increased mechanical interlocking.[80] However, with plasma treatments, the functionalization of the surface in regards to the activation of bonding sites by increasing the wettability and surface energy is understood to lose its effectiveness over time.[78, 79] Therefore, this treatment would have to be done and immediately followed by application of the adhesive layer posing potential challenges to the logistics of the encapsulation process. Furthermore, while inducing roughness to the surfaces of the barrier films may enhance adhesion and subsequently the mechanical stability of the encapsulation, considering the effects to the barrier performance should be thoroughly investigated.

Thus, employing high throughput encapsulation processing via gravure roll coating should be considered as the most promising solution to achieving uniform and defect free encapsulation. Preprocessing of the surface conditions of the barrier films may enhance the adhesion strength and mechanical stability of the bond. However, further testing is required to understand the optimal processing and conditions of the adhesive and barrier films to enable reliable and robust flexible encapsulation.

4.4 Other materials and testing capabilities

This investigation solely considered the performance of a commercial multilayer barrier film combined with various commercial barrier adhesives. Exploring the viability of other barrier material and their performance under bending and peeling stresses may reveal additional findings not considered in this study. Prior to the selection and use of the barrier film, initial fabrication and experimentation was done in attempts to reproduce the promising results demonstrated by Gaume et Al's polymer clay nanocomposite films.[47] As discussed in 1.1.3, PNCs utilize low cost and naturally occurring materials such as montmorillonite (MMT) clay. By dispersing MMT clay in a poly vinyl alcohol (PVA) matrix and coating this film onto Polyethylene terephthalate (PET) films, barrier properties adequate for OPV encapsulation can be achieved. Furthermore, nanoclays provide flame retardancy and other unique mechanical properties that have not be extensively explored in application to OPV encapsulation. Optimization of the solution fabrication recipe is needed to achieve similar results of Gaume et al, but applying the PNCs as a coating to commercial barrier films may achieve even better barrier properties and is of interest to explore. Furthermore, other nanofillers such as glass flakes, carbon nanotubes, reduced graphene oxides, or mica clay have been demonstrated to have effect barrier performance.(22, 46, 47, 49, 50) Exploring the integration of these materials and their ability to achieve robust flexibility whilst maintaining high barrier performance is necessary.

The pressure sensitive adhesive material type was not tested in this investigation due to commercial material availability. PSAs have been shown to be compatible with scalable processing methods such as gravure roll coating and are commonly used in industrial flexible OPV applications. (22, 47, 55) The mechanical reliability of PSAs should be evaluated as they demonstrate promising results in the stability of flexible encapsulated OPV applications.

The bending and peeling tests were conducted in ambient lab testing conditions which is testing parameters could be varied to understand the influence of temperature and relative humidity on the mechanical stability of flexible encapsulation. Furthermore, the applicability of PNCs under significantly humid environments may prove to compromise the effectiveness of the barrier performance nanoclays offer. Nanoclays have been demonstrated to swell as they react/absorb permeating moisture which may contribute to the eventual failure of the encapsulation layer.(46, 48) Furthermore, the reactive epoxies, acrylics, and elastomeric rubber utilized in this investigation integrated desiccants or getters to provide a dynamic functionality. Their performance in high moisture content environments may be altered and the stability of their reactive nature could be understood by the optical calcium tests used by Kempe et al in Chapter 1.[52] Therefore, establishing a controlled atmosphere in which the effect of variable atmospheric conditions can be used to further investigate the mechanical stability of barrier films and interfacial adhesives used in flexible encapsulation.

Finally, the use of finite element analysis (FEA) was not considered in this investigation but may be used to interpret or confirm the accuracy of the results from bending and peeling tests. Modeling the flexible encapsulated systems and analyzing them under various stress conditions may be useful in revealing optimal design parameters such as the mechanical properties of the barrier and adhesive materials as well as the thicknesses that govern reliable and robust performance. While the mechanical properties of the adhesive materials were not consistently provided, basic mechanical tests could be conducted to provide the Young's modulus, elongation at break, or ductility of the materials. The coupling of the adhesive and barrier material's mechanical properties ultimately govern the observed results of the bending and peeling tests. Therefore, identifying the mechanical property that most significantly influences the bending and peeling performance of the barrier and adhesive materials is of upmost importance.

REFERENCES

(1) Solomon, S.; Plattner, G. K.; Knutti, R.; Friedlingstein, P. Irreversible Climate Change Due to Carbon Dioxide Emissions. *Proc. Natl. Acad. Sci. U. S. A.* **2009**, *106* (6), 1704–1709. https://doi.org/10.1073/pnas.0812721106.

(2) Ballif, C.; Haug, F. J.; Boccard, M.; Verlinden, P. J.; Hahn, G. Status and Perspectives of Crystalline Silicon Photovoltaics in Research and Industry. *Nat. Rev. Mater.* **2022**, *7* (8), 597–616. https://doi.org/10.1038/s41578-022-00423-2.

(3) Arai, R.; Furukawa, S.; Hidaka, Y.; Komiyama, H.; Yasuda, T. High-Performance Organic Energy-Harvesting Devices and Modules for Self-Sustainable Power Generation under Ambient Indoor Lighting Environments. *ACS Appl. Mater. Interfaces* **2019**, *11* (9), 9259–9264. https://doi.org/10.1021/acsami.9b00018.

(4) Yang, F.; Huang, Y.; Li, Y.; Li, Y. Large-Area Flexible Organic Solar Cells. *npj Flex. Electron.* **2021**, *5* (1), 1–12. https://doi.org/10.1038/s41528-021-00128-6.

(5) Lu, L.; Effendy, M. Application of Organic Photovoltaic Materials (OPV) as Greenhouse Roof Structures: A Review. *J. Agric. Food Eng.* **2020**, *1* (3), 1–5. https://doi.org/10.37865/jafe.2020.0019.

(6) Sun, L.; Fukuda, K.; Someya, T. Recent Progress in Solution-Processed Flexible Organic Photovoltaics. *npj Flex. Electron.* **2022**, *6* (1). https://doi.org/10.1038/s41528-022-00222-3.

(7) Li, X.; Li, P.; Wu, Z.; Luo, D.; Yu, H. Y.; Lu, Z. H. Review and Perspective of Materials for Flexible Solar Cells. *Mater. Reports Energy* **2021**, *1* (1), 100001. https://doi.org/10.1016/j.matre.2020.09.001.

(8) Zhan, L.; Li, S.; Lau, T.-K.; Cui, Y.; Lu, X.; Shi, M.; Li, C.-Z.; Li, H.; Hou, J.; Chen, H. Over 17% Efficiency Ternary Organic Solar Cells Enabled by Two Non-Fullerene Acceptors Working in an Alloy-like Model. *Energy Environ. Sci.* **2020**, *13* (2), 635–645. https://doi.org/10.1039/C9EE03710A.

(9) Zhan, L.; Li, S.; Li, Y.; Sun, R.; Min, J.; Bi, Z.; Ma, W.; Chen, Z.; Zhou, G.; Zhu, H.; Shi, M.; Zuo, L.; Chen, H. Desired Open-Circuit Voltage Increase Enables Efficiencies Approaching 19% in Symmetric-Asymmetric Molecule Ternary Organic Photovoltaics. *Joule* **2022**, *6* (3), 662–675. https://doi.org/https://doi.org/10.1016/j.joule.2022.02.001.

(10) Zhu, L.; Zhang, M.; Xu, J.; Li, C.; Yan, J.; Zhou, G.; Zhong, W.; Hao, T.; Song, J.; Xue, X.; Zhou, Z.; Zeng, R.; Zhu, H.; Chen, C.-C.; MacKenzie, R. C. I.; Zou, Y.; Nelson, J.; Zhang, Y.; Sun, Y.; Liu, F. Single-Junction Organic Solar Cells with over 19% Efficiency Enabled by a Refined Double-Fibril Network Morphology. *Nat. Mater.* **2022**, *21* (6), 656–663. https://doi.org/10.1038/s41563-022-01244-y.

(11) Kaltenbrunner, M.; White, M. S.; Głowacki, E. D.; Sekitani, T.; Someya, T.; Sariciftci, N. S.; Bauer, S. Ultrathin and Lightweight Organic Solar Cells with High Flexibility. *Nat. Commun.* **2012**, *3*, 770. https://doi.org/10.1038/ncomms1772.

(12) Cheng, P.; Zhan, X. Stability of Organic Solar Cells: Challenges and Strategies. *Chem. Soc. Rev.* **2016**, *45* (9), 2544–2582. https://doi.org/10.1039/c5cs00593k.

(13) Mateker, W. R.; McGehee, M. D. Progress in Understanding Degradation Mechanisms and Improving Stability in Organic Photovoltaics. *Adv. Mater.* **2017**, *29* (10). https://doi.org/10.1002/adma.201603940.

(14) Clarke, A. J.; Luke, J.; Meitzner, R.; Wu, J.; Wang, Y.; Lee, H. K. H.; Speller, E. M.; Bristow, H.; Cha, H.; Newman, M. J.; Hooper, K.; Evans, A.; Gao, F.; Hoppe, H.; McCulloch, I.; Schubert, U. S.; Watson, T. M.; Durrant, J. R.; Tsoi, W. C.; Kim, J. S.; Li, Z. Non-Fullerene Acceptor Photostability and Its Impact on Organic Solar Cell Lifetime. *Cell Reports Phys. Sci.* **2021**, *2* (7), 100498. https://doi.org/10.1016/j.xcrp.2021.100498.

(15) Liu, B.; Sun, H.; Lee, J.-W.; Jiang, Z.; Qiao, J.; Wang, J.; Yang, J.; Feng, K.; Liao, Q.; An, M.; Li, B.; Han, D.; Xu, B.; Lian, H.; Niu, L.; Kim, B. J.; Guo, X. Efficient and Stable Organic Solar Cells Enabled by Multicomponent Photoactive Layer Based on One-Pot Polymerization. *Nat. Commun.* **2023**, *14* (1), 967. https://doi.org/10.1038/s41467-023-36413-3.

(16) Jahandar, M.; Prasetio, A.; Lee, C.; Kim, H.; Kim, A. R.; Heo, J.; Kim, Y.; Kim, S.; Lim, D. C. Highly Efficient Flexible Organic Photovoltaic Modules for Sustainable Energy Harvesting under Low-Light Condition via Suppressing Voltage-Drop by Metal-Mediated Cross-Linkable Polymer Interfacial Layer. *Chem. Eng. J.* **2022**, *448*, 137555. https://doi.org/https://doi.org/10.1016/j.cej.2022.137555.

(17) Sun, Y.; Liu, T.; Kan, Y.; Gao, K.; Tang, B.; Li, Y. Flexible Organic Solar Cells: Progress and Challenges. *Small Sci.* **2021**, *1* (5), 2100001. https://doi.org/https://doi.org/10.1002/smsc.202100001.

(18) Juillard, S.; Planes, E.; Matheron, M.; Perrin, L.; Berson, S.; Flandin, L. Mechanical Reliability of Flexible Encapsulated Organic Solar Cells: Characterization and Improvement. *ACS Appl. Mater. Interfaces* **2018**, *10* (35), 29805–29813. https://doi.org/10.1021/acsami.8b06684.

(19) Riede, M.; Spoltore, D.; Leo, K. Organic Solar Cells—The Path to Commercial Success. *Adv. Energy Mater.* **2021**, *11* (1), 2002653. https://doi.org/https://doi.org/10.1002/aenm.202002653.

(20) van der Staaij, F. M.; van Keulen, I. M.; von Hauff, E. Organic Photovoltaics: Where Are We Headed? *Sol. RRL* **2021**, *5* (8), 1–8. https://doi.org/10.1002/solr.202100167.

(21) Zhang, Y.; Samuel, I. D. W.; Wang, T.; Lidzey, D. G. Current Status of Outdoor Lifetime Testing of Organic Photovoltaics. *Adv. Sci.* **2018**, *5* (8), 1800434. https://doi.org/https://doi.org/10.1002/advs.201800434.

(22) Sutherland, L. J.; Weerasinghe, H. C.; Simon, G. P. A Review on Emerging Barrier Materials and Encapsulation Strategies for Flexible Perovskite and Organic Photovoltaics. *Adv. Energy Mater.* **2021**, *11* (34), 1–32. https://doi.org/10.1002/aenm.202101383.

(23) Jørgensen, M.; Norrman, K.; Gevorgyan, S. A.; Tromholt, T.; Andreasen, B.; Krebs, F. C. Stability of Polymer Solar Cells. *Adv. Mater.* **2012**, *24* (5), 580–612. https://doi.org/10.1002/adma.201104187.

(24) Drakonakis, V. M.; Savva, A.; Kokonou, M.; Choulis, S. A. Solar Energy Materials & Solar Cells Investigating Electrodes Degradation in Organic Photovoltaics through Reverse Engineering under Accelerated Humidity Lifetime Conditions. *Sol. Energy Mater. Sol. Cells* **2014**, *130*, 544–550. https://doi.org/10.1016/j.solmat.2014.07.051.

(25) Madogni, V. I.; Kounouhéwa, B.; Akpo, A.; Agbomahéna, M.; Hounkpatin, S. A.; Awanou, C. N. Comparison of Degradation Mechanisms in Organic Photovoltaic Devices upon Exposure to a Temperate and a Subequatorial Climate. *Chem. Phys. Lett.* **2015**, *640*, 201–214. https://doi.org/10.1016/j.cplett.2015.09.023.

(26) Arredondo, B.; Romero, B.; Beliatis, M. J.; Pozo, G.; Martín-martín, D.; Blakesley, J. C.; Dibb, G.; Krebs, F. C.; Gevorgyan, S. A.; Castro, F. A. Solar Energy Materials and Solar Cells Analysing Impact of Oxygen and Water Exposure on Roll-Coated Organic Solar Cell Performance Using Impedance Spectroscopy. *Sol. Energy Mater. Sol. Cells* **2018**, *176* (October 2017), 397–404. https://doi.org/10.1016/j.solmat.2017.10.028.

(27) Majid, I.; Ahmad Nayik, G.; Mohammad Dar, S.; Nanda, V. Novel Food Packaging Technologies: Innovations and Future Prospective. *J. Saudi Soc. Agric. Sci.* **2018**, *17* (4), 454–462. https://doi.org/https://doi.org/10.1016/j.jssas.2016.11.003.

(28) Fan, Z.; De Bastiani, M.; Garbugli, M.; Monticelli, C.; Zanelli, A.; Caironi, M. Experimental Investigation of the Mechanical Robustness of a Commercial Module and Membrane-Printed Functional Layers for Flexible Organic Solar Cells. *Compos. Part B Eng.* **2018**, *147*, 69–75. https://doi.org/https://doi.org/10.1016/j.compositesb.2018.04.007.

(29) Aitola, K.; Gava Sonai, G.; Markkanen, M.; Jaqueline Kaschuk, J.; Hou, X.; Miettunen, K.; Lund, P. D. Encapsulation of Commercial and Emerging Solar Cells with Focus on Perovskite Solar Cells. *Sol. Energy* **2022**, *237*, 264–283. https://doi.org/https://doi.org/10.1016/j.solener.2022.03.060.

(30) Ahmad, J.; Bazaka, K.; Anderson, L. J.; White, R. D.; Jacob, M. V. Materials and Methods for Encapsulation of OPV: A Review. *Renew. Sustain. Energy Rev.* **2013**, *27*, 104–117. https://doi.org/https://doi.org/10.1016/j.rser.2013.06.027.

(31) Cros, S.; de Bettignies, R.; Berson, S.; Bailly, S.; Maisse, P.; Lemaitre, N.; Guillerez, S. Definition of Encapsulation Barrier Requirements: A Method Applied to Organic Solar Cells. *Sol. Energy Mater. Sol. Cells* **2011**, *95*, S65–S69. https://doi.org/https://doi.org/10.1016/j.solmat.2011.01.035.

(32) Dameron, A. A.; Davidson, S. D.; Burton, B. B.; Carcia, P. F.; McLean, R. S.; George, S. M. Gas Diffusion Barriers on Polymers Using Multilayers Fabricated by Al2O3 and Rapid SiO2 Atomic Layer Deposition. *J. Phys. Chem. C* **2008**, *112* (12), 4573–4580. https://doi.org/10.1021/jp076866+.

(33) Dunkel, R.; Bujas, R.; Klein, A.; Horndt, V. Method of Measuring Ultralow Water Vapor Permeation for OLED Displays. *Proc. IEEE* **2005**, *93* (8), 1478–1482. https://doi.org/10.1109/JPROC.2005.851494.

(34) Graff, G. L.; Williford, R. E.; Burrows, P. E. Mechanisms of Vapor Permeation through Multilayer Barrier Films: Lag Time versus Equilibrium Permeation. *J. Appl. Phys.* **2004**, *96* (4), 1840–1849. https://doi.org/10.1063/1.1768610.

(35) Boldrighini, P.; Fauveau, A.; Thérias, S.; Gardette, J. L.; Hidalgo, M.; Cros, S. Optical Calcium Test for Measurement of Multiple Permeation Pathways in Flexible Organic

Optoelectronic Encapsulation. *Rev. Sci. Instrum.* **2019**, *90* (1), 14710. https://doi.org/10.1063/1.5021182.

(36) Zhang, X. D.; Lewis, J. S.; Parker, C. B.; Glass, J. T.; Wolter, S. D. Measurement of Reactive and Condensable Gas Permeation Using a Mass Spectrometer. *J. Vac. Sci. Technol. A* **2008**, *26* (5), 1128–1137. https://doi.org/10.1116/1.2952453.

(37) Ranade, A.; D'Souza, N. A.; Wallace, R. M.; Gnade, B. E. High Sensitivity Gas Permeability Measurement System for Thin Plastic Films. *Rev. Sci. Instrum.* **2004**, *76* (1), 13902. https://doi.org/10.1063/1.1823792.

(38) Paetzold, R.; Winnacker, A.; Henseler, D.; Cesari, V.; Heuser, K. Permeation Rate Measurements by Electrical Analysis of Calcium Corrosion. *Rev. Sci. Instrum.* **2003**, *74* (12), 5147–5150. https://doi.org/10.1063/1.1626015.

(39) Choi, J. H.; Kim, Y. M.; Park, Y. W.; Huh, J. W.; Ju, B. K.; Kim, I. S.; Hwang, H. N. Evaluation of Gas Permeation Barrier Properties Using Electrical Measurements of Calcium Degradation. *Rev. Sci. Instrum.* **2007**, *78* (6), 64701. https://doi.org/10.1063/1.2747168.

(40) Song, E. H.; Park, Y. W.; Choi, J. H.; Park, T. H.; Jeong, J. W.; Choi, H. J.; Ju, B. K. The Flexible Ca-Test: An Improved Performance in a Gas Permeability Measurement System. *Rev. Sci. Instrum.* **2011**, *82* (5), 54702. https://doi.org/10.1063/1.3584903.

(41) Kempe, M. D.; Reese, M. O.; Dameron, A. A. Evaluation of the Sensitivity Limits of Water Vapor Transmission Rate Measurements Using Electrical Calcium Test. In *Review of Scientific Instruments*; 2013; Vol. 84. https://doi.org/10.1063/1.4789803.

(42) Lu, Q.; Yang, Z.; Meng, X.; Yue, Y.; Ahmad, M. A.; Zhang, W.; Zhang, S.; Zhang, Y.; Liu, Z.; Chen, W. A Review on Encapsulation Technology from Organic Light Emitting Diodes to Organic and Perovskite Solar Cells. *Adv. Funct. Mater.* **2021**, *31* (23). https://doi.org/10.1002/adfm.202100151.

(43) Lay, E.; Wuu, D.-S.; Lo, S.-Y.; Horng, R.-H.; Wei, H.-F.; Jiang, L.-Y.; Lee, H.-U.; Chang, Y.-Y. Permeation Barrier Coatings by Inductively Coupled Plasma CVD on Polycarbonate Substrates for Flexible Electronic Applications. *Surf. Coatings Technol.* **2011**, *205* (17), 4267–4273. https://doi.org/https://doi.org/10.1016/j.surfcoat.2011.03.037.

(44) Khenkin, M. V, Katz, E. A., Abate, A. *et al*. Consensus Statement for Stability Assessment and Reporting for Perovskite Photovoltaics Based on ISOS Procedures. *Nat. Energy* **2020**, *5* (1), 35–49. https://doi.org/10.1038/s41560-019-0529-5.

(45) Channa, I. A.; Distler, A.; Zaiser, M.; Brabec, C. J.; Egelhaaf, H.-J. Thin Film Encapsulation of Organic Solar Cells by Direct Deposition of Polysilazanes from Solution. *Adv. Energy Mater.* **2019**, *9* (26), 1900598. https://doi.org/https://doi.org/10.1002/aenm.201900598.

(46) de Azeredo, H. M. C.; Mattoso, L. H. C.; McHugh, T. H. Nanocomposites in Food Packaging – A Review. In *Advances in Diverse Industrial Applications of Nanocomposites*; Reddy, B., Ed.; IntechOpen: Rijeka, 2011. https://doi.org/10.5772/14437.

(47) Gaume, J.; Taviot-Gueho, C.; Cros, S.; Rivaton, A.; Thérias, S.; Gardette, J. L. Optimization of PVA Clay Nanocomposite for Ultra-Barrier Multilayer Encapsulation of Organic Solar Cells. *Sol. Energy Mater. Sol. Cells* **2012**, *99*, 240–249. https://doi.org/10.1016/j.solmat.2011.12.005.

(48) Seethamraju, S.; Ramamurthy, P. C.; Madras, G. Flexible Poly(Vinyl Alcohol-Co-Ethylene)/Modified MMT Moisture Barrier Composite for Encapsulating Organic Devices. *RSC Adv.* **2013**, *3* (31), 12831–12838. https://doi.org/10.1039/c3ra41557k.

(49) Kopanati, G. N.; Seethamraju, S.; Ramamurthy, P. C.; Madras, G. A Surlyn/Magnesium Oxide Nanocomposite as an Effective Water Vapor Barrier for Organic Device Encapsulation. *RSC Adv.* **2015**, *5* (41), 32580–32587. https://doi.org/10.1039/C5RA03356J.

(50) Yuwawech, K.; Wootthikanokkhan, J.; Tanpichai, S. Functionalized Graphene Nanoplatelets as a Barrier Enhancing Filler in Organic Photovoltaic Encapsulant. *J. Appl. Polym. Sci.* **2021**, *138* (18), 50351. https://doi.org/https://doi.org/10.1002/app.50351.

(51) Weerasinghe, H. C.; Vak, D.; Robotham, B.; Fell, C. J.; Jones, D.; Scully, A. D. New Barrier Encapsulation and Lifetime Assessment of Printed Organic Photovoltaic Modules. *Sol. Energy Mater. Sol. Cells* **2016**, *155*, 108–116. https://doi.org/10.1016/j.solmat.2016.04.051.

(52) Kempe, M. D.; Dameron, A. A.; Reese, M. O. Evaluation of Moisture Ingress from the Perimeter of Photovoltaic Modules. *Prog. Photovoltaics Res. Appl.* **2014**, *22* (11), 1159–1171. https://doi.org/10.1002/pip.2374.

(53) Choi, E. Y.; Kim, J.; Lim, S.; Han, E.; Ho-Baillie, A. W. Y.; Park, N. Enhancing Stability for Organic-Inorganic Perovskite Solar Cells by Atomic Layer Deposited Al2O3 Encapsulation. *Sol. Energy Mater. Sol. Cells* **2018**, *188*, 37–45. https://doi.org/https://doi.org/10.1016/j.solmat.2018.08.016.

(54) Wang, H.; Zhao, Y.; Wang, Z.; Liu, Y.; Zhao, Z.; Xu, G.; Han, T.-H.; Lee, J.-W.; Chen, C.; Bao, D.; Huang, Y.; Duan, Y.; Yang, Y. Hermetic Seal for Perovskite Solar Cells: An Improved Plasma Enhanced Atomic Layer Deposition Encapsulation. *Nano Energy* **2020**, *69*, 104375. https://doi.org/https://doi.org/10.1016/j.nanoen.2019.104375.

(55) Hösel, M.; Søndergaard, R. R.; Jørgensen, M.; Krebs, F. C. Comparison of UV-Curing, Hotmelt, and Pressure Sensitive Adhesive as Roll-to-Roll Encapsulation Methods for Polymer Solar Cells. *Adv. Eng. Mater.* **2013**, *15* (11), 1068–1075. https://doi.org/https://doi.org/10.1002/adem.201300172.

(56) Savagatrup, S.; Printz, A. D.; O'Connor, T. F.; Zaretski, A. V; Rodriquez, D.; Sawyer, E. J.; Rajan, K. M.; Acosta, R. I.; Root, S. E.; Lipomi, D. J. Mechanical Degradation and Stability of Organic Solar Cells: Molecular and Microstructural Determinants. *Energy Environ. Sci.* **2015**, *8* (1), 55–80. https://doi.org/10.1039/C4EE02657H.

(57) Dauskardt, R. H.; Lane, M.; Ma, Q.; Krishna, N. Adhesion and Debonding of Multi-Layer Thin Film Structures. *Eng. Fract. Mech.* **1998**, *61* (1), 141–162. https://doi.org/https://doi.org/10.1016/S0013-7944(98)00052-6.

(58) Sun, Y.; Meng, L.; Wan, X.; Guo, Z.; Ke, X.; Sun, Z.; Zhao, K.; Zhang, H.; Li, C.; Chen, Y. Flexible High-Performance and Solution-Processed Organic Photovoltaics with Robust Mechanical Stability. *Adv. Funct. Mater.* **2021**, *31* (16), 2010000. https://doi.org/https://doi.org/10.1002/adfm.202010000.

(59) Bulusu, A.; Singh, A.; Wang, C. Y.; Dindar, A.; Fuentes-Hernandez, C.; Kim, H.; Cullen, D.; Kippelen, B.; Graham, S. Engineering the Mechanical Properties of Ultrabarrier Films Grown by Atomic Layer Deposition for the Encapsulation of Printed Electronics. *J. Appl. Phys.* **2015**, *118* (8), 85501. https://doi.org/10.1063/1.4928855.

(60) ASTM Standard D1876-08, 2015, "Standard Test Method for Peel Resistance of Adhesives (T-Peel Test)," ASTM International, West Conshohocken, PA, 2015, DOI: 10.1520/D1876-08R15E01, www.astm.org

(61) Landau, L. D.; Lifšic, E. M.; Lifshitz, E. M.; Kosevich, A. M.; Pitaevskii, L. P. *Theory of Elasticity: Volume 7*; Elsevier, 1986; Vol. 7.

(62) Khaund, A. K.; Nicholson, P. S. Fracture of a Brittle Composite: Influence of Elastic Mismatch and Interfacial Bonding. *J. Mater. Sci.* **1980**, *15* (1), 177–187. https://doi.org/10.1007/BF00552443.

(63) Hutchinson, J. W. Stresses and Failure Modes in Thin Films and Multilayers; 1996.

(64) Al-Ramahi, N. J.; Joffe, R.; Varna, J. Criteria for Crack Path Deviation in Adhesive Layer of Bi-Material DCB Specimen. *Compos. Part A Appl. Sci. Manuf.* **2021**, *147*, 106408. https://doi.org/https://doi.org/10.1016/j.compositesa.2021.106408.

(65) Wyser, Y.; Pelletier, C.; Lange, J. Predicting and Determining the Bending Stiffness of Thin Films and Laminates. *Packag. Technol. Sci.* **2001**, *14* (3), 97–108. https://doi.org/https://doi.org/10.1002/pts.540.

(66) Rośkowicz, M.; Godzimirski, J.; Komorek, A.; Jasztal, M. The Effect of Adhesive Layer Thickness on Joint Static Strength. *Mater. (Basel, Switzerland)* **2021**, *14* (6). https://doi.org/10.3390/ma14061499.

(67) Banea, M. D.; da Silva, L. F. M.; Campilho, R. D. S. G. The Effect of Adhesive Thickness on the Mechanical Behavior of a Structural Polyurethane Adhesive. *J. Adhes.* **2015**, *91* (5), 331–346. https://doi.org/10.1080/00218464.2014.903802.

(68) Booth, R. E.; Schrickx, H. M.; Hanby, G.; Liu, Y.; Qin, Y.; Ade, H.; Zhu, Y.; O'Connor, B. T. Silver Nanowire Composite Electrode Enabling Highly Flexible, Robust Organic Photovoltaics. *Sol. RRL* **2022**, *6* (9), 2200264. https://doi.org/https://doi.org/10.1002/solr.202200264.

(69) Kim, J.-H.; Lee, I.; Kim, T.-S.; Rolston, N.; Watson, B. L.; Dauskardt, R. H. Understanding Mechanical Behavior and Reliability of Organic Electronic Materials. *MRS Bull.* **2017**, *42* (2), 115–123. https://doi.org/DOI: 10.1557/mrs.2017.3.

(70) Brand, V.; Bruner, C.; Dauskardt, R. H. Cohesion and Device Reliability in Organic Bulk Heterojunction Photovoltaic Cells. *Sol. Energy Mater. Sol. Cells* **2012**, *99*, 182–189. https://doi.org/https://doi.org/10.1016/j.solmat.2011.11.035.

(71) Li, S.; Liu, X.; Li, R.; Su, Y. Shear Deformation Dominates in the Soft Adhesive Layers of the Laminated Structure of Flexible Electronics. *Int. J. Solids Struct.* **2017**, *110–111*, 305–314. https://doi.org/https://doi.org/10.1016/j.ijsolstr.2016.12.006.

(72) Gent, A. N.; Hamed, G. R. Peel Mechanics of Adhesive Joints. *Polym. Eng. Sci.* **1977**, *17* (7), 462–466. https://doi.org/https://doi.org/10.1002/pen.760170708.

(73) Bartlett, M. D.; Case, S. W.; Kinloch, A. J.; Dillard, D. A. Peel Tests for Quantifying Adhesion and Toughness: A Review. *Prog. Mater. Sci.* **2023**, *137*, 101086. https://doi.org/https://doi.org/10.1016/j.pmatsci.2023.101086.

(74) Śliwa-Wieczorek, K.; Zając, B. Rigid and Flexible Double Shear Lap Adhesive Joint at Elevated Temperature-An Experimental Study. *Polymers (Basel).* **2021**, *13* (17). https://doi.org/10.3390/polym13172873.

(75) Blackman, B. R. K.; Kinloch, A. J.; Rodriguez Sanchez, F. S.; Teo, W. S.; Williams, J. G. The Fracture Behaviour of Structural Adhesives under High Rates of Testing. *Eng. Fract. Mech.* **2009**, *76* (18), 2868–2889. https://doi.org/https://doi.org/10.1016/j.engfracmech.2009.07.013.

(76) Kanninen, M. F. Applications of Dynamic Fracture Mechanics for the Prediction of Crack Arrest in Engineering Structures. *Int. J. Fract.* **1985**, *27* (3), 299–312. https://doi.org/10.1007/BF00017974.

(77) Andrews, E. H.; Kinloch, A. J.; Melville, H. W. Mechanics of Adhesive Failure. II. Proc. R. Soc. London. A. Math. Phys. Sci. 1997, 332 (1590), 401–414. https://doi.org/10.1098/rspa.1973.0033.

(78) Hegemann, D.; Brunner, H.; Oehr, C. Plasma Treatment of Polymers for Surface and Adhesion Improvement. *Nucl. Instruments Methods Phys. Res. Sect. B Beam Interact. with Mater. Atoms* **2003**, *208*, 281–286. https://doi.org/https://doi.org/10.1016/S0168-583X(03)00644-X.

(79) Berczeli, M.; Weltsch, Z. Enhanced Wetting and Adhesive Properties by Atmospheric Pressure Plasma Surface Treatment Methods and Investigation Processes on the Influencing Parameters on HIPS Polymer. *Polymers (Basel).* **2021**, *13* (6). https://doi.org/10.3390/polym13060901.

(80) van Dam, J. P. B.; Abrahami, S. T.; Yilmaz, A.; Gonzalez-Garcia, Y.; Terryn, H.; Mol, J. M. C. Effect of Surface Roughness and Chemistry on the Adhesion and Durability of a Steel-Epoxy Adhesive Interface. *Int. J. Adhes. Adhes.* **2020**, *96*, 102450. https://doi.org/https://doi.org/10.1016/j.ijadhadh.2019.102450.

APPENDICES

Delo Photobond LP 4415

TECHNICAL DATASHEET

DELO® PHOTOBOND® LP4115

modified acrylate | 1C | UV- / VIS-curing

high water vapor barrier

Special features of product

- compliant with RoHS Directive 2015/863/EU

Typical area of use

- -40 - 120 °C

Curing

Suitable lamp types	LED 365 nm, LED 400 nm	
Typical irradiation time *intensity 200 mW/cm²* *LED 400 nm* *layer thickness 100 µm*	4	s

Processing

Storage life in unopened original container *at +18 °C to +25 °C*	6	month(s)

Technical properties

Color in uncured condition	yellowish
Transparency	transparent
Color in cured condition in 0.1 mm layer thickness	colorless
Color in cured condition in 1 mm layer thickness	colorless

Parameters

Density *DELO Standard 13 | liquid*	0.9	g/cm³
Viscosity *by the criteria of DIN EN 12092 | liquid | Rheometer | Shear rate: 10 1/s*	1800	mPa·s
Compression shear strength *DELO Standard 5 | **Glass** | **Glass** | 400 nm | 200 mW/cm² | 60 s*	4	MPa

Compression shear strength *DELO Standard 5 / **PMMA** / **PMMA** / 400 nm / 200 mW/cm² / 60 s*	2	MPa
Peel resistance *DELO Standard 34 / **PC** / **PC** / 400 nm / 200 mW/cm² / 60 s*	0.6	N/mm
Peel resistance *DELO Standard 34 / **PET** / **PET** / 400 nm / 200 mW/cm² / 60 s*	1.4	N/mm
Tensile strength *by the criteria of DIN EN ISO 527 / 400 nm / 150 mW/cm² / 90 s*	2	MPa
Elongation at tear *by the criteria of DIN EN ISO 527 / 400 nm / 150 mW/cm² / 90 s*	460	%
Shore hardness A *by the criteria of DIN EN ISO 868 / 400 nm / 200 mW/cm² / 90 s*	18	
Glass transition temperature *DMTA / 400 nm / 200 mW/cm² / 60 s*	31	°C
Shrinkage *DELO Standard 13 / 400 nm / 200 mW/cm² / 60 s*	5.2	vol. %
Water absorption *by the criteria of DIN EN ISO 62 / 400 nm / 200 mW/cm² / 60 s / Type of storage: Media / Medium: Distilled water / Storage temperature: at approx. +23 °C*	0.1	wt. %
Permeation *by the criteria of ASTM E 96 / Layer thickness: 300 µm / 400 nm / 200 mW/cm² / 60 s / Type of storage: Constant climate / Storage temperature: 60 °C / Humidity: 90 % / Duration: 24 h*	12	(g·mm)/(m²·24h)

Converting table

°F	= (°C x 1.8) + 32	1 MPa	= 145.04 psi
1 inch	= 25.4 mm	1 GPa	= 145.04 ksi
1 mil	= 25.4 µm	1 cP	= 1 mPa·s
1 oz	= 28.3495 g	1 N	= 0.225 lb

General curing and processing information

The curing time stated in the technical data was determined in the laboratory. It can vary depending on the adhesive quantity and component geometry and is therefore a reference value.Increasing or decreasing the curing temperature and / or irradiation intensity and / or irradiation time shortens or prolongs the curing time and can lead to changed physical properties.All curing or light fixation parameters depend on material thickness and absorption, adhesive layer thickness, lamp type and distance between lamp and adhesive layer.Values measured after 24 h at approx. 23 °C / 50 % r.h., unless otherwise specified.

Delo Katiobond LP655

TECHNICAL DATASHEET

DELO

DELO® KATIOBOND® LP655

modified epoxy resin | 1C | UV- / VIS-curing

free of solvents | thixotropic | high water vapor barrier

Special features of product
- compliant with RoHS Directive 2015/863/EU

Typical area of use
- -40 - 120 °C

Curing

Suitable lamp types	LED 365 nm, LED 400 nm, UVA	
Minimum irradiation dose *LED 400 nm*	2000	mW·s/cm²
Typical irradiation time *intensity 200 mW/cm²* *LED 400 nm*	20	s
Typical curing time *at rt approx. + 23 °C* *irradiated*	24	h

Processing

Typical adhesive application	needle dispensing	
Conditioning time (typical) *when stored in cold conditions* *in containers up to 1,000 ml*	6	h
when stored in cold conditions *in containers up to 10 l*	12	h
Processing time *at rt approx. +23 °C*	28	d
Storage life in unopened original container *at 0 °C to +10 °C*	6	month(s)

DELO

Technical properties

Transparency	translucent
Color in cured condition in 0.1 mm layer thickness	colorless
Transparency in cured condition in 0.1 mm layer thickness	transparent
Color in cured condition in 1 mm layer thickness	yellowish

Parameters

Density *DELO Standard 13 | liquid*	1.38	g/cm³
Viscosity *liquid | Rheometer | Shear rate: 10 1/s*	12000	mPa·s
Thixotropy index *liquid | Rheometer*	1.3	
Maximum curable layer thickness *DELO Standard 20 | **White substrate** | 400 nm | 200 mW/cm² | 20 s | Plus | at approx. +23 °C | 24 h*	0.4	mm
Maximum curable layer thickness *DELO Standard 20 | **White substrate** | 400 nm | 200 mW/cm² | 60 s | Plus | at approx. +23 °C | 24 h*	0.7	mm
Compression shear strength *DELO Standard 5 | **Glass** | **Al** | 400 nm | 200 mW/cm² | 20 s | Plus | at approx. +23 °C | 24 h*	12	MPa
Compression shear strength *DELO Standard 5 | **Glass** | **Glass** | 400 nm | 200 mW/cm² | 20 s | Plus | at approx. +23 °C | 24 h*	9	MPa
Compression shear strength *DELO Standard 5 | **Glass** | **PC** | 400 nm | 200 mW/cm² | 20 s | Plus | at approx. +23 °C | 24 h*	3	MPa
Tensile strength *by the criteria of DIN EN ISO 527 | 400 nm | 200 mW/cm² | 60 s | Plus | at approx. +23 °C | 24 h*	22	MPa
Elongation at tear *by the criteria of DIN EN ISO 527 | 400 nm | 200 mW/cm² | 60 s | Plus | at approx. +23 °C | 24 h*	1	%
Young's modulus *DMTA | 400 nm | 200 mW/cm² | 60 s | Plus | at approx. +23 °C | 24 h | Type of storage: Temp. | Storage temperature: 205 °C | Duration: 30 min*	5300	MPa
Shore hardness D *by the criteria of DIN EN ISO 868 | 400 nm | 200 mW/cm² | 60 s | Plus | at approx. +23 °C | 24 h*	84	

Glass transition temperature *DMTA / 400 nm / 200 mW/cm² / 60 s / Plus / at approx. +23 °C / 24 h / Type of storage: Temp. / Storage temperature: 205 °C / Duration: 30 min*	183	°C
Coefficient of linear expansion *DELO Standard 26 / TMA / Evaluation T: 30 °C - 40 °C / 400 nm / 200 mW/cm² / 60 s / Plus / at approx. +23 °C / 24 h*	45	ppm/K
Coefficient of linear expansion *DELO Standard 26 / TMA / Evaluation T: 140 °C - 150 °C / 400 nm / 200 mW/cm² / 60 s / Plus / at approx. +23 °C / 24 h*	132	ppm/K
Shrinkage *DELO Standard 13 / 400 nm / 200 mW/cm² / 60 s / Plus / at approx. +23 °C / 24 h*	2.4	vol. %
Permeation *Layer thickness: 300 µm / 400 nm / 200 mW/cm² / 20 s / Plus / at approx. +23 °C / 24 h / Type of storage: Constant climate / Storage temperature: 60 °C / Humidity: 90 % / Duration: 24 h*	6	(g·mm)/(m²·24h)
Relative permittivity *1 MHz*	3.1	
Relative permittivity *10 MHz*	3.2	
Relative permittivity *100 MHz*	3.1	
Relative permittivity *1000 MHz*	3	

Converting table

°F	= (°C x 1.8) + 32	1 MPa	= 145.04 psi
1 inch	= 25.4 mm	1 GPa	= 145.04 ksi
1 mil	= 25.4 µm	1 cP	= 1 mPa·s
1 oz	= 28.3495 g	1 N	= 0.225 lb

General curing and processing information

The curing time stated in the technical data was determined in the laboratory. It can vary depending on the adhesive quantity and component geometry and is therefore a reference value.Increasing or decreasing the curing temperature and / or irradiation intensity and / or irradiation time shortens or prolongs the curing time and can lead to changed physical properties.All curing or light fixation parameters depend on material thickness and absorption, adhesive layer thickness, lamp type and distance between lamp and adhesive layer.Curing until final strength proceeds within 24 hours at room temperature.High temperatures during or after curing can lead to post-crosslinking of the adhesive which influences the physical properties of the bond.Values measured after 24 h at approx. 23 °C / 50 % r.h., unless otherwise specified.

Everlight 313

Eversolar® AB-313

Spec.	Results
Main composition	Resin / Oligomer
Appearance	Transparent viscous liquid
Viscosity (mPas) @28℃ NDJ 8S、Spindle size 4、12 RPM	38,000± 8,000
Curing condition LED 365nm Thickness:1mm	9J/cm²
Absorption wavelength	360-365nm 、405nm
Tensile strength Glass/Glass	≧50Kg/cm²
WVTR (40℃/90%RH) / Thickness:200um	≦6.5 g/m²•24hrs
Storage environment	Dark and room temperature

AB-313

1. For dispensing and screen printing
2. High transparency
3. Solvent-free
4. Yellowing resistance
5. Room temperature storage

5

Everlight Chemical

Everlight 341

Eversolar® AB-341

Spec.	Result
Main composition	Resin / Oligomer
Appearance	Gray viscous liquid
Viscosity (mPas) @25℃	40,000±10,000
Curing condition LED 365nm Thickness:1mm	9J/cm²
Absorption wavelength	360-365nm 、405nm
Tensile strength Glass/Glass	≧30Kg/cm²
WVTR (40℃/90%RH) / Thickness:200um	<1g/m²•24hrs
Storage environment	Dark and room Temperature

AB-341

1. For dispensing and screen printing
2. Opaque or non-transparency
3. High moisture penetration resistance
4. Solvent-free
5. Yellowing resistance
6. Room temperature storage

6

Everlight Chemical

ADCO SOLAR

Product Information

HelioSeal™ PVS 101

Reactive/Desiccated Solar Edge Sealant

Description

HelioSeal™ PVS 101 is a synthetic polymer based sealant with integrated desiccant for dehydrating the airspace in photovoltaic and thermal module constructions. Unlike traditional solar edge sealants, HelioSeal™ PVS 101 provides exceptional adhesion to glass surfaces in addition to providing an excellent barrier to water vapor and gas permeation.
HelioSeal™ PVS 101 can be used as a single seal in EVA or thermoplastic encapsulated photovoltaic modules.

HelioSeal™ PVS 101 offers the following benefits over other edge sealing products

Features	Benefits
Optimum adhesion to glass	Superior module life
Good adhesion to common module substrates	Can be used for a variety of frontsheet / backsheet combinations
Very low water vapor and gas permeability	Maximum protection for water sensitive components
Very good UV resistance	Long module life, improved lifetime output
Modules meet UL 1703, IEC 61215 and IEC 61646	Proven performance in demanding applications
High productivity due to fully automated application	Can be applied either as tape or dispensed from bulk
UL Listed	Listed under QIHE2 - Photovoltaic Polymeric Materials - Component

Packaging

220 kg drum also available as a tape in custom dimensions

Consult Material Safety Data Sheet (MSDS) before using.

Technical Information	
Base	Synthetic polymer, solvent free
Color	Black
Consistency	Tape or bulk compound, recommended dispensing temperature of 110°C -157°C (230°F - 315°F)
Stability	Functionality over a large range of temperatures from -40°C - 90°C (-40°F - 194°F)
Density	1.35 g/cm³
MVTR	< 0.01 g/m² · day
Volume Resistivity	> 10^{10} Ohm · cm

Shelf Life Properties

Storage	Store in tightly closed drums or sealed metalized bags if in extruded form.
Shelf-life	At least 9 months when stored unopened in original packaging

Basic Use

The surfaces must be dry, clean and free from dust and grease. Suitable glass washing machines must be used for cleaning glass substrates.

HelioSeal™ PVS 101 is supplied in a "ready-to-use" state but must be heated to 110°C - 157°C (230°F - 315°F) when dispensed from drum packaging. Additional detailed application instructions for HelioSealTM PVS 101 are available on request.

HelioSeal™ PVS 101 was specially developed for sealing and bonding of photovoltaic and solar thermal panels. Users are advised to confirm adhesion and compatibility of HelioSeal™ PVS 101 to substrates and materials which will come in contact with it before application. Care should be taken with plastics which show a tendency to stress crack. For further information, please contact our Customer Service Department.

CAUTION: All statements and technical information in this document are based on tests or data that ADCO believes is reliable. However, ADCO does not warrant or guarantee the accuracy or completeness of this information. The user has sole knowledge and control of factors that can affect the performance of ADCO's products in the user's intended application. It is the user's responsibility to conduct tests to determine the compatibility of ADCO's product with the design, structure, and materials of the user's end product and the suitability of ADCO's product for the user's method of application and intended use. The user assumes all risk and liability arising out of such use.

P.O. Box 457, 4401 Page Avenue Michigan Center, MI 49254 Phone: (800) 248-4010 Fax: (517) 764-6697 www.adcocorp.com

EVA-B601

American Solar Supply
www.americansolarsupply.com

EVA- B601

EVA （Ethylene Vinyl Acetate Copolymer）is used as the main raw material for EVA film which is for encapsulating solar modules. EVA film is Produced by thermal processing and forming equipment when EVA is fully mixed With some modified accessory ingredients. EVA film is easy to handle for it is inviscid under room temperature. When encapsulating solar modules, the processing requirements should be followed. From bottom to top, we place glass, EVA, solar cell, EVA and TPT(TPE,PET)， then all these will be put in to the preheated Laminator to be laminated and solidified. The solidified solar cell, after being fixed with aluminium alloy frame and terminal box and then being tested and packed, becomes the solar cell module.

1.Laminating and solidifying process conditions:

Solidifying way		Fast solidifying(B601)
Laminating and solidifying	Temperature of hot plates (℃)	138-140
	Time of the creation of vacuum(min)	5
	Time of pressure increasing and keeping(min)	13-15

2.Laminating and solidifying operating instructions:

(1) The laminating process conditions can vary according to the laminator's property. Different laminator may have different laminating process conditions.

(2) The temperature of laminator's working environment is different from laminating temperature, and accordingly, the process conditions are different. Generally speaking, in summer, the time used to create vacuum is shorter than that in winter.

(3) The higher the laminating or solidifying temperature is, the shorter the time will be. Contrarily, the lower the temperature is, the longer the time will be. If the temperature of laminator or curing box is even, relatively higher solidifying temperature can save time and cut cost, and also can increase production efficiency.

CONTACT :
Gehring Corporation 3384 Pennyroyal Rd Franklin, Ohio 45005 937-743-9398

3.Quality Assurance:

- ISO9001
- ISO14001
- SGS
- UL/TUV

4.Laminating curing process condition:

Curing mode		
Laminating curing	Hot-plate temp(℃)	143-145℃
	Vacuum time （min）	5.5Min （-101.3MPa）
	Laminating time （min）	-60KPa 20s -40KPa 10s -20Kpa 600s

5.Product test:

Test Item		Test Standard	Unit	Standard Values	Test Values
Density		ISO1183	g/cm3		0.96
Tensile Strength			MPa	≥15	26
Elongation at break		GBT1040.2-2006	%	≥400	450
Optical Transmission		GBT2410-2008	%		>91
Shrinkage	TD	QB/BJBM-01-2010	%	≤3	<2
	MD		%	≤3	<2
Cross-linking Rate after laminate(143-145 ℃,16min）		QB/BJ-03-152	%	≥75	82-86
Dielectrical strength		GBT1408-2006	Kv/mm		60
Volume Resistance		GBT1410-2006	Ω		$7.8*10^{14}$
Peeling strength	Backsheet	GB/T2790	N/cm	≥60	>80
	Glass			≥40	>80
UV cutoff wavelength		GBT2410-2008	nm		360
Water-absorbing rate		GBT1034-1998	%		0.1

CONTACT :
Gehring Corporation 3384 Pennyroyal Rd Franklin, Ohio 45005 937-743-9398